OPEN ACCESS

Editors' Choice—The Effect of Anchor Group and Alkyl Backbone Chain on Performance of Organic Compounds as Corrosion Inhibitors for Aluminum Investigated Using an Integrative Experimental-Modeling Approach

View the article online for updates and enhancements.

Editors' Choice—The Effect of Anchor Group and Alkyl Backbone Chain on Performance of Organic Compounds as Corrosion Inhibitors for Aluminum Investigated Using an Integrative Experimental-Modeling Approach

I. Milošev,[1,*,z] D. Zimerl,[1] Ch. Carriére,[2] S. Zanna,[2] A. Seyeux,[2] J. Iskra,[1,a]
S. Stavber,[1] F. Chiter,[2] M. Poberžnik,[1] D. Costa,[2] A. Kokalj,[1,z] and P. Marcus[2,**,z]

[1]*Jožef Stefan Institute, Department of Physical and Organic Chemistry, SI-1000 Ljubljana, Slovenia*
[2]*PSL Research University, CNRS—Chimie ParisTech, Institut de Recherche de Chimie Paris (IRCP), Physical Chemistry of Surfaces Group, 75005 Paris, France*

An alkaline etched, superhydrophilic aluminum surface was modified using functionalized alkyl compounds selected to study the effect of their properties on adsorption on the metal surface. The thirteen organic compounds differed in alkyl chain length (eight and eighteen carbon atoms) and anchor group (azide, imidazole, thiocyanate, amino, disulfide, thiol, phosphonic, carboxylic, and benzoic). The methodology of the study integrated a complete chain of steps incorporating synthesis, electrochemical and surface analyses, and computational modeling. The corrosion resistant and superhydrophobic properties depend on the anchor group, which governs adhesion to the surface, and backbone, which is responsible for lateral cohesive interactions. The morphology and chemical composition of modified layers were studied using scanning electron microscopy, X-ray photoelectron spectroscopy and time-of-flight secondary ion mass spectrometry. Electrochemical and long-term immersion properties were investigated in 0.5 M NaCl. Calculations based on density functional theory were performed as to model the adsorption of selected anchor groups on the hydroxylated oxidized aluminum surface. Integrated results allowed the identification of the anchor groups that are able to form inhibitive adsorbed layers on Al surface regardless the alkyl chain length, and those that are not able to form adsorbed layers at all and are thus not efficient corrosion inhibitors.

This is the second part of a three-part series of articles about the organic molecules as corrosion inhibitors for aluminum prepared in such a way as to enable the study of the effect of anchor group (adsorbed on the metal surface) and backbone (responsible for lateral interactions between the adsorbed organic molecules). The methodology is the same in each article of the series and integrates a complete chain of steps, from planning, synthesis, electrochemical and surface analyses to modeling. The integration of versatile methodological approaches enabled us to target the decisive properties of organic molecules that are responsible for adsorption and formation of condensed layers, which show barrier corrosion resistance and superhydrophobicity. The alkaline etched, superhydrophilic aluminum surface was taken as a starting point for further modification of the surface by immersion in an ethanol solution of selected organic compounds. The ground aluminum surface does not allow the study of adsorption of organic molecules due to the naturally formed oxidized layer, which does not have a large tendency for adsorption of organic molecules.[1] In the first part of the study we investigated the effect of chain length for a single carboxylic anchor group.[1] Seven carboxylic acids (CAs) ranging from hexanoic to octadecanoic were investigated.[1] At constant immersion time (30 min) and CA concentration (5 mM), short CAs (CA-6 and CA-7) act as corrosion activators, longer CAs (CA-8, CA-9 and CA-10) act as weak corrosion inhibitors, but only long chain acids (CA-14 and, especially, CA-18) are efficient corrosion inhibitors that also provide barrier protection of Al and show superhydrophobic properties. X-ray photoelectron spectroscopy (XPS) and time-of-flight secondary ion mass spectrometry (ToF-SIMS) analyses corroborated that short and long carboxylic acid

(CA-8 and CA-18) form an adsorbed organic layer. Experimental data obtained on the formation of a carboxylate layer on Al surface were the basis for density functional theory (DFT) modeling. It is proposed that the adsorption proceeds via the condensation mechanism. The magnitude of adsorption energy increases with length of alkyl chains and additionally leads to increased cohesive lateral forces resulting in a more stable molecular film on the surface. Only molecules with a long alkyl chain, like octadecanoic acid, completely cover the surface due to molecular tilting.[1] In the current study, which is the second part of this series, we proceeded to study the effect of various anchor groups and alkyl chain length aiming to bring new insight into the mechanism of formation of protective inhibitor layers on the Al surface and to contribute to a better understanding of surface-organic molecule interactions. This would consequently enable better utilization of predictive capacity of inhibitor performance.

The need for development of environmentally safe and efficient corrosion inhibitors, which would be applicable on different metals, is constantly growing due to legislation which restricts the use of chemical compounds that are proven to have, or may potentially have, a negative impact on the environment and human health. There are several possible routes we can follow to meet these needs: (i) introduce new chemical compounds which are equally or even more efficient than currently used inhibitors,[2] and (ii) use a combination of existing inhibitors whose synergistic action would increase their individual efficiency.[3] When introducing new inhibitors screening, synthesis, up-scaling and rigorous testing is required which must be in accordance with the REACH directive.[4] Screening itself is demanding and requires a large number of trial-and-error experiments. Automated, high-throughput methods of screening accelerate the discovery of new inhibitors and generate large data sets suitable as a basis for further analysis and development of predictive models using machine learning modeling or statistical methods, the so called quantitative structure-activity relationships (QSAR) or quantitative structure-property relationship (QSPR).[2] Descriptors that are usually utilized are structural and physicochemical

*Electrochemical Society Member.
**Electrochemical Society Fellow.
[a]Present address: University of Ljubljana, Faculty of Chemistry and Chemical Technology, Večna pot 113, SI-1000 ljubljana, Slovenia.
[z]E-mail: ingrid.milosev@ijs.si; tone.kokalj@ijs.si; philippe.marcus@chimie-paris-tech.fr

properties as well as molecular electronic parameters such as chemical hardness, electronegativity, energy of the highest occupied (HOMO) and lowest unoccupied (LUMO) molecular orbitals, and the HOMO–LUMO energy gap ($E_{LUMO} - E_{HOMO}$). Such electronic parameters can be routinely calculated with DFT (density-functional-theory) calculations. Furthermore, DFT modeling can also bring information about the molecule−surface interactions as well as the equilibrium adsorption and electronic structures. DFT can also describe bond-breaking and bond-making.[5] Dynamic effects can be addressed with the aid of molecular dynamics (MD) simulations (force-field or DFT-based), which simulate atomic motion at finite temperatures.[6–8] However, it is usually very difficult, or almost impossible, to postulate the correlations for large number of different types of inhibitors.[9] Recently a robust, predictive, quantitative computational model was built which can generate useful predictions.[10] The study pointed out the need for further examination of metal surface-organic inhibitor interactions which would enable more pertinent descriptors at the DFT level and then combine computational modeling with high-throughput experiments.

The organic inhibitors used for aluminum in chloride solutions are numerous, the most commonly used molecules being various azole, mercapto, quinoline and carboxylic derivatives.[11,12] A clear correlation between descriptors and inhibition efficiency is difficult to establish for a large number of different compounds. In the present study we utilized the approach where the inhibitor structure is divided into an anchor group and a backbone. This division allows us to study the effect of the anchor group and the effect of backbone separately. Nine anchor groups were selected either based on our previous studies on different metals[5,9,13–15] or based on literature studies.[11,16–19] It was shown recently that the lateral interactions between the alkyl tails of corrosion inhibitor molecules are important for the formation of adsorbed self-assembled layers on the metal surface, and that the morphology of the adsorbed layers is strongly influenced by molecular geometry.[1,6,20]

It was shown in our previous study that the preparation of the substrate is important, as the ground Al surface covered by native formed oxide film is not suitable for adsorption of organic layers. Instead, the aluminum surface was made superhydrophylic by alkaline etching, resulting in the formation of aluminum hydroxide.[1,21] A series of chemical compounds was chosen in the present work to allow the study of the effect of anchor group on corrosion inhibition performance (Fig. 1). Each chemical compound consists of an alkyl chain with eight (designated as C8) or eighteen carbon atoms (C18) and an anchor group. Nine anchor groups, bonded to the C8 alkyl chain, were investigated: azide, imidazole, thiocyanate, amino, disulfide, thiol, phosphonic, carboxylic and benzoic. Four of these (thiol, imidazole, phosphonic, and carboxylic) were also investigated for the C18 alkyl chain. Scanning electron microscopy combined with energy dispersive X-ray spectrometry (SEM/EDS) were used to analyze the morphology of surfaces. XPS and ToF-SIMS were used for chemical surface analysis following the approach used previously for analysis of conversion coatings on Al alloys.[22,23] In addition to experimental techniques, DFT calculations were used to investigate the adsorption affinity of anchor groups, utilizing the approach from our previous studies.[1,20,24,25] Based on these results it was determined whether a particular organic molecule was bonded to the surface. Protection properties of adsorbed organic layers were studied by electrochemical measurements in NaCl solution. Protection ability was correlated to surface analysis results, i.e. adsorbed molecules enabled a certain degree of inhibition, whilst those which were not adsorbed failed as inhibitors. In addition to electrochemical analysis, the bare etched Al sample and Al samples modified by organic layers were immersed in NaCl solution up to six months and then analyzed.

Experimental

Substrate material.—Aluminum (>99.0%) 1 mm thick flat sheet, distributed by GoodFellow, England, was used as substrate. Samples were cut out in a form of 1 mm thick flat discs with a diameter of 15 mm.

Organic compounds.—Organic compounds used for the formation of adsorbed layers on aluminum were either purchased from commercial suppliers or synthesized in-house.

The following chemicals were purchased: octanoic acid (Alfa Aesar, 98%), nonanoic acid (95%, Fluorochem), 1-octanethiol, (99%, Fluorochem), octylamine (99%, Sigma Aldrich), octylphosphonic acid (98%, Ark Pharm), 4-octylbenzoic acid (98%, Ark Pharm), octadecanoic acid (97%, ACROS organic), 1-octadecanethiol (95%, Fluorochem) and octadecylphosphonic acid (95%, Fluorochem). Octylphosphonic acid, 4-octylbenzoic acid, octadecylphosphonic acid, octadecanoic acid and 1-octadecanethiol are in solid form. All other purchased compounds (octanoic acid, nonanoic acid, 1-octanethiol, and octylamine) are in liquid form.

The following chemicals were used for the in-house synthesis: H_2O_2 (30%, Carlo Erba), ethanol (anhydrous, Carlo Erba), acetonitrile (99.9%, Sigma Aldrich), tetrahydrofuran (99.9%, Sigma Aldrich), dimethyl formamide (99.7%, Merck), imidazole (99.5%, Sigma Aldrich), 1-iodooctane (98%+, Alfa Aesar), 1-iodooctadecane (98%, Fluorochem), KI (99.5%, Merck), diethyl ether (99.8%, Sigma Aldrich), anhydrous Na_2SO_4 (99.5%, Fisher Chemicals), NaN_3 (99%, Riedel-de Haën), KSCN (99%, Sigma Aldrich), NaOH (p.a., Labochem International), dichloromethane (99.5%, J.T. Baker), $Na_2S_2O_3$ (99.5%, Merck).

Synthesis and characterization.—Octyl azide (C8-N_3) was synthesized from NaN_3 (2.76 g, 42 mmol) and 1-iodooctane (1.71 g, 7 mmol) stirred at 60 °C in dimethylformamide (35 ml).[26] The reaction mixture was followed by thin liquid chromatography (TLC); silica gel on TLC foils was used with fluorescence indicator 254 nm and pore size 60 Å. After 20 h, the substrate peak disappeared and water was added to the reaction mixture and extracted with diethyl ether (3 × 50 ml). The combined organic phase was washed with water (3 × 50 ml) to remove remaining dimethylformamide, dried over anhydrous Na_2SO_4 and evaporated under reduced pressure to give octyl azide (1.02 g, 6.6 mmol, 94% yield) as a colorless oil.

N-octylimidazole (C8-ImiH) was synthesized according to the following modified procedure[27]: to a solution of imidazole (0.816 g, 12 mmol) in 10 ml acetonitrile (MeCN), NaOH (2 g, 50 mmol) was added, and stirred for 30 min. After that time, 1-iodooctane (1.48 g, 6 mmol) in 10 ml acetonitrile was added and the reaction mixture was heated to 80 °C. The progress of the reaction was followed by TLC. After 12 h the substrate peak disappeared and the solvent evaporated, the crude reaction mixture was dissolved in dichloromethane and washed with water (3 × 50 ml), dried over anhydrous Na_2SO_4 and evaporated under reduced pressure. The evaporated extract was purified by column chromatography (ethyl acetate: ethanol 7:3) and the combined fractions were evaporated under reduced pressure to give N-octylimidazole (0.811 g, 4.5 mmol, 75% yield) as a yellow oily liquid.

Octyl thiocyanate (C8-SCN) was synthesized from 1-iodooctane (1.71 g, 7 mmol) and KSCN (2.06 g, 21 mmol) refluxed in tetrahydrofuran (20 ml).[28,29] The reaction was followed by TLC. After 20 h, peak for substrate disappeared and water was added to the reaction mixture and extracted with dichloromethane (3 × 15 ml). The combined organic phase was dried over anhydrous Na_2SO_4 and evaporated under reduced pressure to give octyl thiocyanate (1.17 g, 6.85 mmol, 98% yield) as a yellow oil.

For the synthesis of dioctyl disulphide (C8-SS-C8), KI (0.013 g, 0.08 mmol) and 30% hydrogen peroxide (0.907 ml, 8.8 mmol) were added to a solution of octane thiol (1.39 ml, 8 mmol) in ethanol (10 ml).[30,31] The progress of the reaction was followed by TLC. After 2 h, the substrate peak disappeared and sat. aq. $Na_2S_2O_3$ (15 ml) was added to use the remaining hydrogen peroxide. The reaction mixture was extracted with dichloromethane (3 × 20 ml). The combined organic phase was washed with water (1 × 25 ml) and
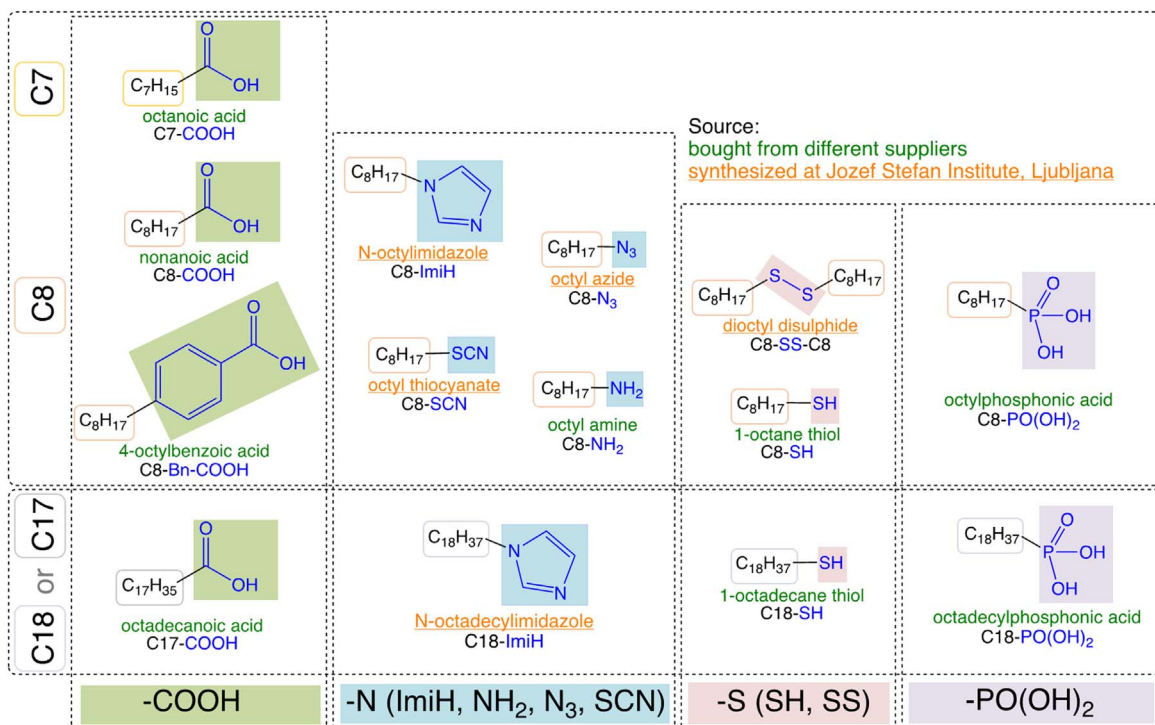
Figure 1. Skeletal and chemical formulae of octyl and octadecyl organic compounds with different anchor groups used as potential corrosion inhibitors for etched aluminum. Compounds were either synthesized in our laboratory (denoted orange) or purchased (denoted green). Synthetic routes are described in Experimental and presented in Fig. 2. Anchor groups are color labeled: green for carbon containing compounds (carboxylic COOH and benzoic Bn-COOH), blue for nitrogen containing (azide N_3, amino NH_2, and imidazole ImiH), red for sulfur containing (thiol SH, disulfide SS, and thiocyanate SCN), and violet for phosphorus containing (phosphonic $PO(OH)_2$).

dried over anhydrous Na_2SO_4 solvent evaporated under reduced pressure to give dioctyl disulphide (1.14 g, 3.9 mmol, 98% yield) as a yellow oil.

For the synthesis of N-octadecylimidazole (C18–ImiH), NaOH (2 g, 25 mmol) was added to a solution of imidazole (0.408 g, 6 mmol) in 10 ml acetonitrile, and stirred for 30 min.[27,32] After that time, 1-iodooctadecane (1.16 g, 3 mmol) in 15 ml acetonitrile was added and the reaction mixture was heated to 80 °C. The progress of the reaction mixture was followed by TLC. After 12 h, the substrate peak disappeared and the solvent was evaporated, the crude reaction mixture was dissolved in dichloromethane and washed with water (3 × 50 ml), dried over anhydrous Na_2SO_4 and evaporated under reduced pressure. The evaporated extract was purified by column chromatography (ethyl acetate: ethanol 7:3), the combined fractions were evaporated under reduced pressure to give N-octadecylimidazole (0.682 g, 2.1 mmol, 71% yield) as yellow waxy crystals.

Liquid-state ^{1}H and ^{13}C nuclear magnetic resonance (NMR) spectra were recorded to evaluate the conversion of substrate to final product and purity of synthesized compounds after selected purification method. NMR spectra were recorded on Bruker Avance III 500 instrument at 25 °C. Chemical shifts (δ) are shown in ppm using $CDCl_3$ as internal standard for [1]H (δH 7.27 ppm) and for [13]C (δC 77.00) spectra. Samples were dissolved in $CDCl_3$, tetramethyl silane (TMS) was added for internal reference. Conversion of substrate to final product was calculated as quotient between the integrals of selected peaks for substrate and finished product. For peak integration, MestReNova 11.0.0 was used. The final yield of synthesis was calculated as a ratio between practical yield and theoretical yield (based on stoichiometry of reaction) expressed as percentage.

Substrate pre-treatment and preparation of adsorbed organic layers.—Aluminum samples were first ground under water using SiC papers up to 2400-grit (LaboPol, Struers) and etched in alkaline NaOH solution (p.a., Labochem International).[1,21] Briefly, 20 ml 0.1 M NaOH was heated in a flat-bottomed flask (volume 250 ml)

using an ISOPAD® heater up to 90 °C. The aluminum samples were then immersed in NaOH solution and heated for 20 min at 90 °C. The samples were then cooled down for 45 min in the same solution to room temperature and rinsed by ethanol. This procedure was used in our previous study.[1]

Organic layers were prepared by immersion of etched Al samples in ethanol solution (absolute for analysis EMSURE®) of organic chemicals at room temperature. The concentration of organic compounds was 5 mM and time of immersion was 30 min. The samples were hung in a glass vessel containing ethanol solution using a Teflon thread. After 30 min immersion, the sample was taken out, rinsed by distilled water, dried in a stream of N_2 and used for further measurements.

Samples prepared by etching in NaOH and coated by immersion in ethanol solution of organic chemical are referred to as "Cx-R," where Cx denotes an n-alkyl chain consisting of x carbon atoms and R is the abbreviation of the anchor group (Fig. 1): carboxylic (COOH), azide (N_3), imidazole (ImiH), disulphide (SS), thiol (SH), amino (NH_2), thiocyanate (SCN), phosphonic ($PO(OH)_2$) and benzoic (Bn-COOH).

Characterization methods.— *Electrochemical measurements.*— To record potentiodynamic polarization curves, a three-electrode cell (K0235 Flat Cell Kit, volume 250 ml Ametek, Berwyn, PA, USA) was used. Electrochemical measurements were performed in 0.5 M NaCl, pH = 5.8 (Honeywell Fluka, 99.5%) at room temperature.

A specimen ("Al" or "Cx-R") embedded in a Teflon holder leaving an area of 1.0 cm² exposed to the solution served as the working electrode. A silver/silver chloride (Ag/AgCl, 0.205 V vs standard hydrogen electrode) was used as the reference electrode and a platinum mesh as the counter electrode. Potentials in the text refer to the Ag/AgCl scale. Measurements were conducted using an Autolab potentiostat/galvanostat Model 204 (Utrecht, The Netherlands). Prior to measurements, the sample was allowed to rest under open circuit conditions for approximately 1 h, to reach a stable, quasi-steady state

open circuit potential (E_{oc}) at the end of the stabilization period. Following stabilization, the potentiodynamic polarization curves were recorded using a 1 mV s^{-1} potential scan rate, starting 250 mV more negative with respect to E_{oc}, and then increased in the anodic direction. For each sample, measurements were performed at least in triplicate. Mean values with standard deviations are given in tables and representative measurement was chosen to be presented in graphs. The corrosion potential (E_{corr}) and the corrosion current density (j_{corr}) were obtained from an intercept between cathodic and anodic curves, or by extrapolation of linear portion of the cathodic Tafel curve and the intersect with line passing through E_{corr}.

Immersion test.—Immersion tests were carried out in 250 ml glass vials at room temperature (25 ± 2 °C). Samples were hung in the vial using a teflon thread. The test lasted either one or six months. After the denoted immersion time, the sample was taken out, rinsed by distilled water, dried in a stream of N_2 and used for further measurements.

Water drop contact angle.—Contact angles (θ) were determined using a tensiometer Krüss DSA 20 (Krüss GmbH, Hamburg, Germany). The θ values were measured based on the image of the deionized water drop with a volume of 8–10 μl on the sample surface, using drop-shape-analysis software which enables the fitting of the water drop shape and a precise determination of the contact angle. Each value is the average of at least three measurements made at different locations on the same sample. Mean values with standard deviations are given. In general, $\theta \leqslant 10°$ are regarded as super-hydrophilic, $10° \langle \theta \rangle 90°$ hydrophilic, $90° \langle \theta \rangle 150°$ hydrophobic and $\theta \geqslant 150°$ superhydrophobic.[33]

Surface morphology and composition.—The morphology and composition of modified samples were characterized using the (i) field-emission SEM (FE-SEM), JSM 7600F, JEOL, Japan, equipped with EDS (Inca Oxford 350 EDS SDD); images were recorded at an energy of 5 kV in LEI (low secondary electron image) mode and (ii) FE-SEM Helios Nanolab 650 microscope; images were recorded at an energy of 2 kV in secondary electron mode (SE). Prior to analysis, the samples were sputter-coated with a thin Au layer.

Time-of-flight secondary ion mass spectrometry measurements were performed using a dual beam ToF-SIMS V spectrometer (ION-TOF GmbH, Muenster, Germany). The base pressure in the analysis chamber is maintained at less than 5.0 · 10^{-9} mbar in normal operating conditions. The total primary ion flux was less than 10^{12} ions cm^{-2} ensuring static conditions. A Bi$^+$ primary ion source with a 1.2 pA current, scanned over a 100 × 100 μm^2 area was used as the analysis beam. 2D spectra of negatively charged ions were recorded. Each sample was analyzed at least twice on different areas of the sample. Data acquisition and processing were performed using the IonSpec software. The exact mass values of at least five known species were used for calibration of the data.

X-ray Photoelectron Spectroscopy analysis was performed using Thermo Electron Escalab 250 spectrometer. A monochromated Al Kα X-ray source ($h\nu$ 1486.6 eV) was used. The base pressure in the analytical chamber was maintained at 10^{-9} mbar. The spectrometer was calibrated using Au 4f$_{7/2}$ at 84.1 eV. The take-off angle was 90° and the analyzed area was a 500 μm diameter disk. Survey spectra were recorded with a pass energy of 100 eV at a step size of 1 eV and high resolution spectra of the C 1s, P 2p, N 1s and S 2p core level regions were recorded with a pass energy of 20 eV at a step size of 0.1 eV. The values of the photoionization cross-sections (σ_X) at 1486.6 eV were taken from Scofield,[34] and the inelastic mean free paths (λ_X^Y) were calculated by the TPP2M formula.[35]

Computational details.—Calculations were performed with the PWscf code from the Quantum ESPRESSO distribution,[36,37] using the generalized gradient approximation (GGA) of Perdew–Burke–Ernzerhof (PBE).[38] We used the pseudopotential method with

ultrasoft pseudopotentials.[39,40] To better describe lateral intermolecular interactions within the adsorbed layer, the D2 dispersion correction of Grimme was used.[41] Since Al ions in the oxide film are practically devoid of electrons (they are in a +3 oxidation state), the C_6 parameter of Al was set to zero. This reparametrization will be denoted as PBE-D$_0$, where the subscript "0" is used as mnemonic to recall that C_6 of Al is zero. Kohn–Sham orbitals were expanded in a plane-wave basis set up to a kinetic energy cutoff of 35 Ry (280 Ry for the charge density). Brillouin zone integrations were performed with the special point technique using a Methfessel–Paxton smearing of 0.03 Ry.[42] Molecular graphics were produced by the XCRYSDEN graphical package.[43]

Two models of the hydroxylated oxidized aluminum surface are taken from our previous publications and are described in greater detail therein.[1,20,25,44] The majority of calculations were performed with the first model, designated as OH/Al$_x$O/Al(111), which is based on oxidizing the Al(111) surface with the equivalent of 2 monolayer (ML) of oxygen atoms as proposed by Lanthony et al.[45] The topmost layer of the film is then fully hydroxylated; the corresponding density of surface hydroxyls is 7.1 OH nm^{-2}. The model employed in this study is built from a 6 layer slab of Al(111). Calculations were performed in a (4 × 4) supercell of Al(111) and a 3 × 3 × 1 k-point grid with the previously obtained bulk lattice parameter of 4.04 Å. For the second model the (010) surface of gibbsite Al(OH)$_3$ was taken. The utilized Al(OH)$_3$(010) surface model consists of two discrete Al(OH)$_3$ multilayers interlinked with H bonds.[44] It has the surface hydroxyl density of 13.4 OH nm^{-2}. Adsorption was modeled with a (2 × 1) supercell of Al(OH)$_3$(010) using a shifted 2 × 2 × 1 k-mesh.

The reaction energy (ΔE), was calculated as:

$$\Delta E = E_{products} - E_{reactants} = \sum_i^{products} E_i - \sum_j^{reactants} E_j, \qquad [1]$$

where the energies were calculated at 0 K, without the zero point energy correction. The Gibbs free energies (G) were calculated at a finite temperature of 298 K (with zero-point energy (ZPE) included) following the approach described in our previous publication.[25] To make the vibrational calculations of surface models feasible with our computational resources, the calculations were performed with a single k-point. Furthermore, the OH/Al$_x$O/Al(111) model was simplified by reducing the thickness of the Al support to two Al (111) layers. According to our convergence tests these simplifications are acceptable.[44] All degrees of freedom were relaxed and vibrational frequencies were evaluated at the Γ q-point, by using the PHonon code[46] from the Quantum ESPRESSO distribution.[36,37] To correct for the breakdown of the harmonic oscillator model at low-frequencies, the quasi harmonic approximation of Cramer–Truhlar[47] was applied such that the frequencies below 100 cm^{-1} were raised to 100 cm^{-1}. In the case of standalone molecules, the contributions arising from translation and rotation were taken into account by means of the ideal-gas approximation and the rigid rotor model, respectively. The free energy was therefore calculated as:

$$G(T, p) = E_0 + E_{trv}(T) + pV - TS_{trv}(T, p), \qquad [2]$$

where E_0 is the Kohn–Sham total energy at 0 K, without the zero-point correction, whereas $E_{trv}(T)$ and $S_{trv}(T, p)$ are the translational-rotational-vibrational thermal energy (with ZPE included) and entropy, respectively. For surfaces and adsorbates only the vibrational contributions were taken into account whereas the pV term was neglected, i.e.:

$$G(T) \approx E_0^{full} + E_{vib}^{red}(T) - TS_{vib}^{red}(T), \qquad [3]$$

where E_0^{full} is the total energy at 0 K of the full slab model, whereas E_{vib}^{red} and S_{vib}^{red} are the vibrational thermal energy (with ZPE included) and entropy calculated with the computationally-reduced slab model, respectively. The reaction ΔG is then calculated analogously to Eq. 1.

Results and Discussion

Synthesis of organic compounds.—The basic idea of this study was to investigate the effect of various anchor groups at a constant alkyl chain length on the affinity of adsorption on the Al surface. Nine anchor groups were selected: carboxylic (COOH), benzoic (Bn–COOH), thiocyanate (SCN), azide (N_3), amino (NH_2), imidazole (ImiH), thiol (SH), disulfide (SS) and phosphonic ($PO(OH)_2$). Two lengths of carbon chains were selected, octyl (C8) and octadecyl (C18). Altogether thirteen compounds were investigated. Their skeletal formulae, chemical names and abbreviations are depicted in Fig. 1. Anchor groups are color labelled: blue for nitrogen containing (N_3, NH_2, and ImiH), red for sulfur containing (SH, SS, and SCN), violet for phosphorus containing ($PO(OH)_2$) and green for carbon containing (COOH and Bn-COOH) groups. Please note that there are two exceptions from the described labelling: (i) XPS and ToF–SIMS analyses were carried out on octanoic acid (C7-COOH) instead of nonanoic acid (C8-COOH); electrochemical data were obtained from C8-COOH, and (ii) octadecanoic acid (C17-COOH) was regarded in the C18 group (and not nonadecanoic acid (C18-COOH) as would be required following the postulated labelling) and both surface analysis and electrochemical data refer to this compound.

For the shorter C8-chain, all nine groups were investigated: six compounds were purchased from commercial suppliers ($C8-PO(OH)_2$, C8-SH, C7-COOH/C8-COOH, $C8-NH_2$ and C8-Bn-COOH), and four were synthesized (C8-N_3, C8-SCN, C8-SS-C8 and C8-ImiH). The synthesis of these compounds is described in the Experimental section and schematically shown in Fig. 2. Briefly, octyl azide and octyl thiocyanate were synthesized from octyl iodide using NaN_3 and KSCN as reagents, respectively. Dioctyl disulfide was synthesized from octane thiol and H_2O_2 and N-octylimidazole from imidazole and 1-iodooctane. All synthesized compounds are in liquid form. Their NMR spectra are presented in the Supplement material (Figs. S1–S4 is available online at stacks.iop.org/JES/167/061509/mmedia) and are in accordance with literature data for organic azide,[26] disulfide,[31,48] imidazole[27] and thiocyanate.[29,49]

For the longer C18-chain, four anchor groups (COOH, $PO(OH)_2$, SH and ImiH) were selected, based on the results obtained for the shorter C8-chain (Fig. 1). Three compounds were purchased from commercial suppliers ($C18-PO(OH)_2$, C18-SH, C17-COOH), whereas C18-ImiH was synthesized from imidazole and 1-iodooctadecane, following a similar procedure as for C8-ImiH. The NMR spectrum for these yellow waxy crystals is presented in Fig. S5 and is consistent with literature data.[50]

Morphology and composition of etched aluminum modified with alkyl compounds with various anchor groups.—The etched Al surface shows a micro- and nanoscopically rough surface covered with aluminum hydroxide as proved by EDS, XPS and ToF–SIMS.[1] The surface roughness is ca. 8 μm.[1] Two main morphologies of aluminum hydroxide are observed: platelet-like, nanometer-sized bottom layer and micrometer-sized oblong cones consisting of micro and sub-micrometer sized terraced, pyramidal-like structure (Fig. 3a). Such a surface is superhydrophilic.

After immersion in ethanol solution of alkyl compounds of nine anchor groups, the hierarchical morphology was not disturbed and the surface remained virtually unchanged. An example is given in Fig. 3b for etched Al immersed in $C8-PO(OH)_2$. It is noteworthy that in repetitive samples the surface morphology of alkaline etched Al was never completely the same as the growth of the cones occurs during the cooling phase in NaOH.[1] This will be shown by some examples below. The presence of an organic layer could not be detected using SEM/EDS as the thickness of organic layers was in the nanometer region unsuitable for EDS analysis.

Additionally, the surface wettability of various samples was measured. The as-prepared bare etched Al surface was superhydrophilic. After immersion in ethanol solution, the surface wettability remained superhydrophilic for most of the investigated compounds (Table I). The wettability changed to hydrophobic for C8-Bn-COOH and to superhydrophobic for C18-COOH, $C8-PO(OH)_2$ and $C18-PO(OH)_2$. The change in wettability due to the elongation of the alkyl chain from 8 to 18 was therefore the most
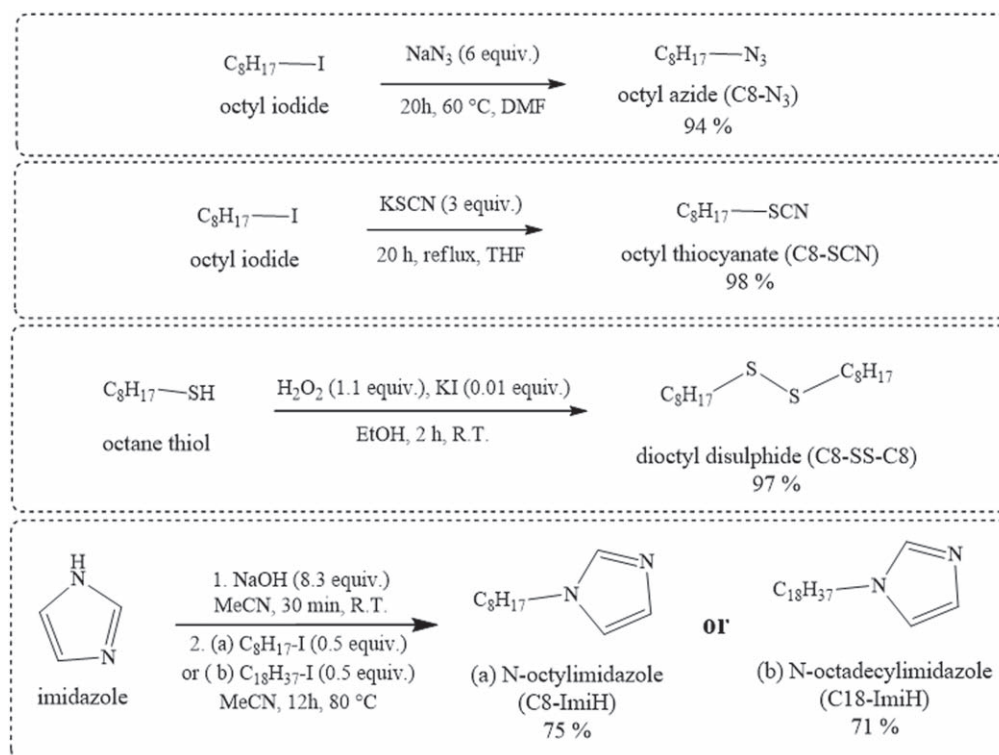

Figure 2. Synthesis routes for octyl azide, octyl thiocynate, dioctyl disulphide, N-octylimidazole and N-octadecylimidazole.
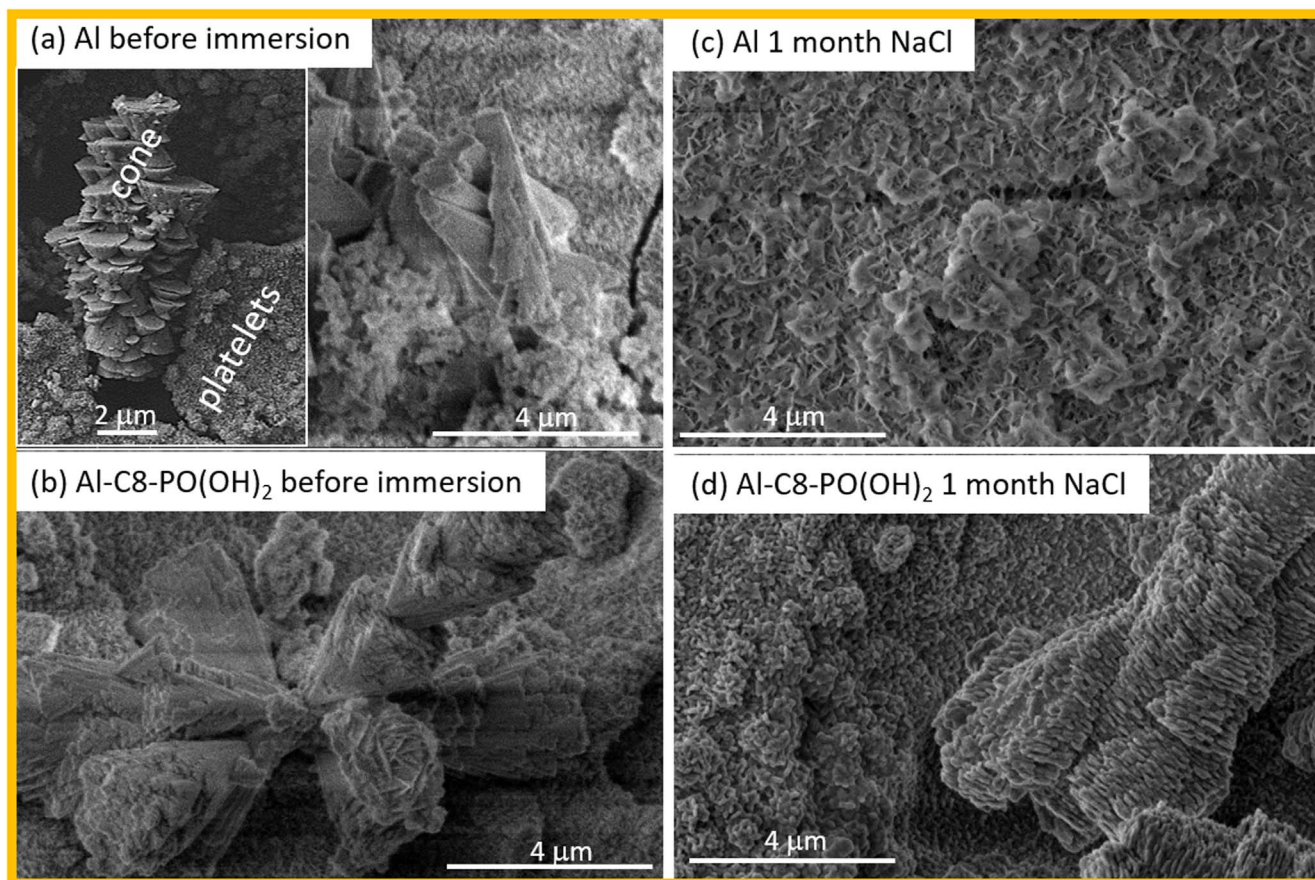
Figure 3. SEM images recorded at the surface of (a), (c) bare etched Al and (b), (d) etched Al sample modified by C8-PO(OH)$_2$ (a), (b) before and (c), (d) after immersion in 0.5 M NaCl for 1 month. After preparation, the sample was cut in half; one half was then immersed in 0.5 M NaCl; therefore, the same sample was imaged before and after immersion in NaCl. The bare Al surface was superhydrophilic before and after immersion; C8-PO(OH)$_2$-modified surface was superhydrophobic before immersion and hydrophobic (a mean contact angle of 105°) after immersion. SE images were recorded at 5 kV and magnification 5,000×.

extreme for the carboxylic group, going from superhydrophilic to superhydrophobic. Regardless the chain length the surface was superhydrophobic for the phosphonic group and superhydrophilic for thiol and imidazole anchor groups.

XPS analysis was performed on Al after etching in 0.1 M NaOH and immersion for 30 min in 5 mM ethanol solution of C8-R (Fig. 4). High resolution N 1s XPS spectra recorded on the Al etched surface exposed to anchor groups containing nitrogen, C8-SCN, C8-NH$_2$, C8-N$_3$ and C8-ImiH, are shown in Fig. 4a. No peak was observed on the spectra meaning that no nitrogen was detected on the etched Al surface. Similarly, high resolution S 2p XPS spectra

recorded on the Al etched surface exposed to different anchor groups containing sulfur, C8-SCN, C8-SH, C8-SS-C8, C18-SH, are shown in Fig. 4b. No peak was observed meaning that these molecules were not present on the surface to a sufficient extent taking into account the sensitivity of XPS analysis of 1 at%.[51] In contrast, a peak at 134.8 eV was detected in the P 2p high resolution spectra recorded for the C8-PO(OH)$_2$ sample (Fig. 5a) associated with the presence of phosphonate groups on the Al etched surface. As for the C7-COOH sample, two peaks were observed in the high resolution C 1s core level: one peak at 285 eV associated to C–C, C–H bonds and the second one at 289.3 eV characteristic for the COOH group,

Table I. Wettability of the surface of bare alkaline etched aluminum (labelled as Al) and etched aluminum covered by an organic layer (labelled as Cx–R) where x is the number of carbon atoms in the alkyl chain ($x = 8$ or 18) and R is the anchor group as defined in Fig. 1. Al was etched for 20 min in 0.1 M NaOH at 90 °C, cooled down in the same solution, and then immersed in 5 mM ethanol solution of the organic chemical.

| Sample	Wettability	Sample	Wettability
Al	superhydrophilic		
C8-N$_3$	superhydrophilic		
C8-SS-C8	superhydrophilic		
C8-COOH	superhydrophilic	C17-COOH	superhydrophobic
C8-Bn-COOH	hydrophobic		
C8-SCN	superhydrophilic		
C8-SH	superhydrophilic	C18-SH	superhydrophilic
C8-NH$_2$	superhydrophilic		
C8-ImiH	superhydrophilic	C18-ImiH	superhydrophilic
C8-PO(OH)$_2$	superhydrophobic	C18-PO(OH)$_2$	superhydrophobic
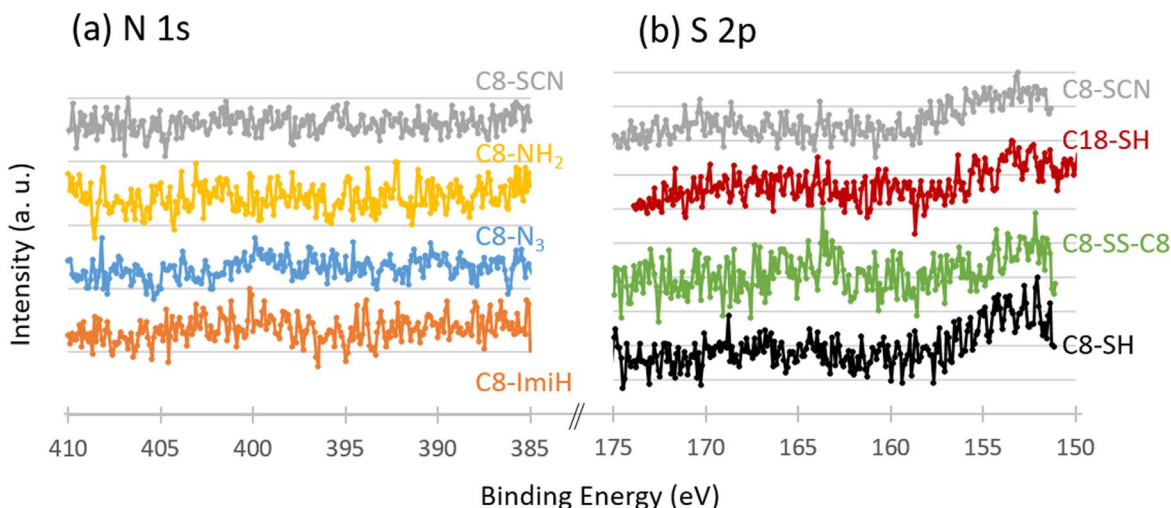
Figure 4. XPS high energy resolution spectra of (a) N 1s and (b) S 2p obtained on alkaline etched Al immersed for 30 min in 5 mM ethanol solution of C8-SCN, C8-NH$_2$, C8-N$_3$, C8-ImiH, C8-SH, C8-SS-C8 and C18-SH.

confirming the presence of the C7-COOH molecule on the Al etched surface (Fig. 5b), as already reported in our previous study (in which it was also shown that the layer coverage was incomplete for this molecule).[1]

It is interesting to note that elongating the alkyl chain from C8 to C18 does not change the result for Cx-COOH and Cx-PO(OH)$_2$. In particular, XPS peaks characteristic of molecules are observed, meaning that molecules are bonded to the surface. Indeed, a peak at 134.8 eV associated with the phosphonate group is observed on the P

2p core level spectra for both Cx-PO(OH)$_2$ samples. Additionally, a peak at 289.3 eV, associated with the COOH group, is detected on the C1s core level of Cx-COOH and C8-Bn-COOH samples (Fig. 5).

It can be concluded that COOH and PO(OH)$_2$ anchor groups are bonded to the Al etched surface, whereas the other tested anchor groups, containing nitrogen or sulfur, are not present on the surface in a sufficient amount.

Long-term stability of organic layers on etched Al modified with alkyl compounds with different anchor groups was investigated
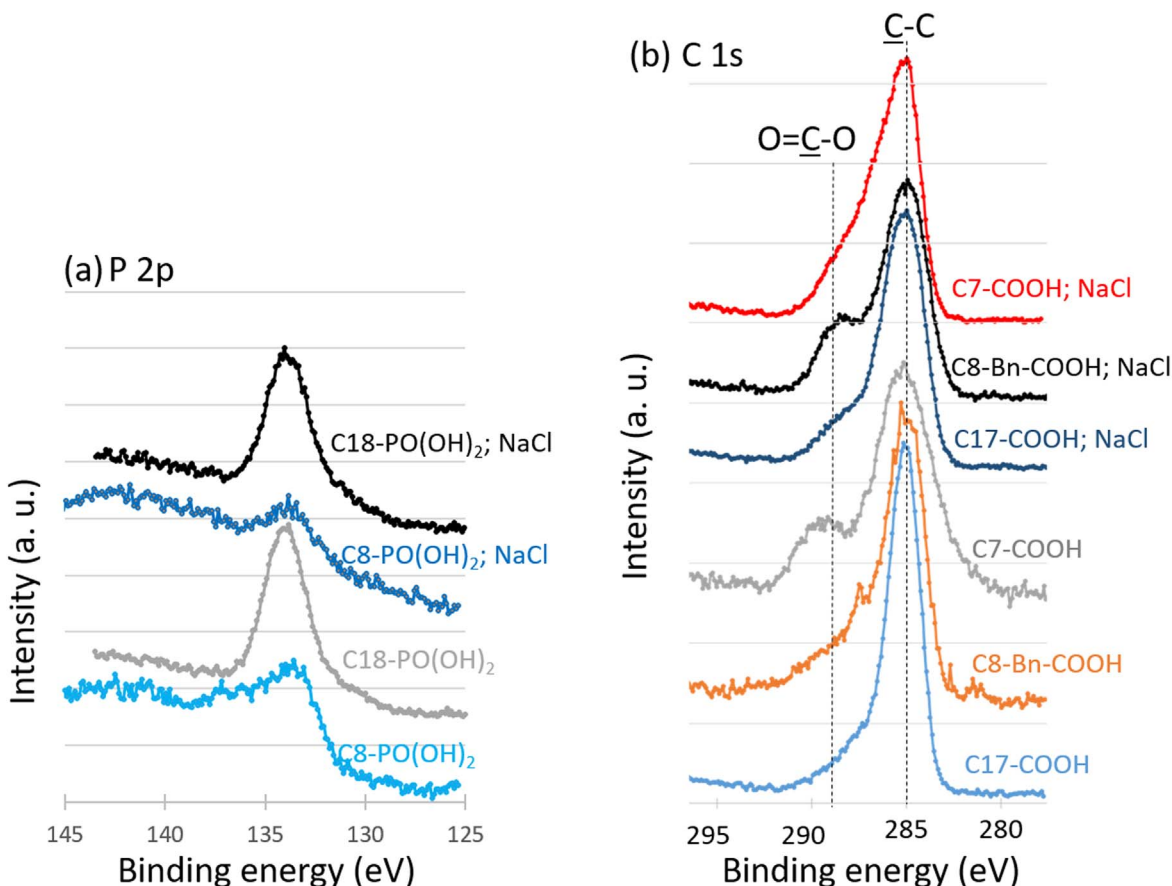

Figure 5. XPS high energy resolution spectra of (a) P 2p and (b) C 1s obtained on alkaline etched Al immersed for 30 min in 5 mM ethanol solution of C7-COOH, C17-COOH, C8-Bn-COOH, C8-PO(OH)$_2$, C18-PO(OH)$_2$ before and after immersion in 0.5 M NaCl (denoted NaCl) for 6 months for all samples except C18-PO(OH)$_2$ which was immersed for 1 month.

through long-term (1 or 6 months) immersion in 0.5 M NaCl. Firstly, bare alkaline etched Al and Al modified with C8-PO(OH)$_2$ were compared before (i.e. as-prepared samples) and after immersion in 0.5 M NaCl. Alkaline etched Al exhibits a hierarchical micro- and nanostructure of Al hydroxide (Fig. 3a). This superhydrophilic structure changed after long-term immersion in NaCl with cones progressively transformed into platelets (Fig. 3c). The surface remained superhydrophilic. SEM images of the surface of C8-PO(OH)$_2$ modified alkaline etched Al sample before and after immersion in NaCl for 1 month are given in Figs. 3b and 3d. In contrast to bare etched Al, the hierarchical pattern was preserved even after 1 month immersion. XPS P 2p spectra confirmed the presence of the phosphonic group indicating that organic molecules were still bonded on the Al surface (Fig. 5a). The surface of C8-PO(OH)$_2$ sample was initially superhydrophobic, while after 1 month immersion it became hydrophobic with a mean contact angle of 123°.

It is noteworthy that alkaline etching in NaOH always produced a hierarchical structure but not necessarily displaying the same morphology. Figure 6 presents an example of surface morphology of alkaline etched Al samples modified with octyl and octadecyl compounds with different anchor groups after six months immersion in 0.5 M NaCl. Upon immersion, the morphology remained hierarchical; for several samples the shape of surface features changed indicating the formation of a thicker layer similar to the phosphonic layer in Fig. 3d. The following surfaces were superhydrophilic before and after the test: C8-N3, C8-ImiH, C8-SS-C8, C8-SCN, C8-SH and C7-COOH. The surface of C8-Bn-COOH was hydrophobic, and that of C17-COOH and C8-PO(OH)$_2$ superhydrophobic before the test and hydrophobic after six months (mean contact angle of 113° and 106° for C17-COOH and C8-PO(OH)$_2$, respectively). XPS analyses were performed on immersed C8-PO(OH)$_2$, C18-PO(OH)$_2$, C7-COOH, C17-COOH, C8-Bn-COOH after long term immersion in NaCl (6 months for all samples except C18-PO(OH)$_2$ which was immersed for 1 month). Figure 5 presents the high resolution C 1s core level on C7-COOH, C17-COOH and C8-Bn-COOH samples and the high resolution P 2p core level recorded on C8-PO(OH)$_2$ and C18-PO(OH)$_2$ samples. The peak at 134.8 eV associated with phosphonates on C8-PO(OH)$_2$ and C18-PO(OH)$_2$ samples is still present, meaning that molecules are still bonded to the surface even after the six months immersion in NaCl. For C7-COOH, C17-COOH, and C8-Bn-COOH, the peak at 289.3 eV on the C 1s core level, characteristic of the COOH group, is still present for all immersed samples. It can be concluded that C8-PO(OH)$_2$, C18-PO(OH)$_2$, C7-COOH, C17-COOH and C8-Bn-COOH molecules are still bonded to the Al etched surface even after immersion in NaCl. For example, the quantity of phosphonic-based inhibitor at the surface can be estimated from the intensity ratio of P 2p and Al 2p peaks. This ratio is 0.078 before the as-prepared (prior to NaCl immersion) for C8-PO(OH)$_2$ and 0.035 after 6 months immersion in NaCl, i.e. 45% of the inhibitor is still present on the surface after immersion. For C18-PO(OH)$_2$, the ratio is 0.342 before and 0.215 after 1 month immersion, i.e., 63% of the inhibitor is still bonded.

These results point out that the surface morphology and topography are necessary but not decisive factors in the strength of adsorption of organic molecules. The hierarchical surface was not necessarily related to wettability, because wettability also depends on the chemical composition of the adsorbed layer. It is noteworthy that a rough etched surface is required for organic molecules to adsorb, because none of the molecules adsorbed on the ground Al surface.[1] This implies that proper surface preparation is essential for effective molecular adsorption. Our results further indicate that the anchor group plays a more decisive role in the formation of a stable adsorbed layer than the alkyl chain length. Molecules which were able to adsorb strongly on the Al surface were detected by XPS and acted as strong inhibitors (phosphonic group for C8 and C18 chains and carboxylic group for C17 chain). These molecules remained adsorbed for a prolonged period of time, indicating strong adsorption. Others (N$_3$, ImiH, NH$_2$, SS, SCN, SH) were not detected by

XPS and therefore desorbed prior to measurements or were not adsorbed at all. This will be further corroborated in the electrochemical measurements presented below.

ToF-SIMS spectra were recorded on the same Al samples with inhibitors bonded to the surface, as proved by XPS, i.e., R-COOH and R-PO(OH)$_2$. One reference sample (prepared by following the same procedure without any inhibitor) and the five organic compounds, C7-COOH, C17-COOH, C8-Bn-COOH, C8-PO(OH)$_2$ and C18-PO(OH)$_2$ have been tested in this study. The comparison between the ToF-SIMS mass spectra obtained on the reference sample and on the samples exposed to organic inhibitors (Fig. 7) evidences the presence of each compound on the Al surface. In fact, specific and intense fragments, $C_8H_{15}O_2^-$ (m/z = 143), $C_{18}H_{35}O_2^-$ (m/z = 283), $C_{15}H_{21}O_2^-$ (m/z = 233), $C_8H_{18}PO_3^-$ (m/z = 193) and $C_{18}H_{38}PO_3^-$ (m/z = 333), that are assigned to C7-COOH (144 g.mol^{-1}), C17-COOH (284 g.mol^{-1}), C8-Bn-COOH (234 g.mol^{-1}), C8-PO(OH)$_2$ (194 g.mol^{-1}) and C18-PO(OH)$_2$ (334 g.mol^{-1}) respectively, were observed. The detected fragments correspond to the mass of the inhibitor molecule minus one hydrogen, as commonly observed in negative polarity ToF-SIMS.[52] Note that $C_8H_{15}O_2^-$ and $C_{18}H_{35}O_2^-$, indicated with grey background in Fig. 7, had previously been detected by ToF-SIMS and associated with the presence of C7-COOH and C17-COOH, respectively, on the Al surface.[1]

Focusing on C7-COOH and C17-COOH inhibitors, the mass spectra exhibit the characteristic fragments of the inhibitors themselves ($C_8H_{15}O_2^-$ (m/z = 143) and $C_{18}H_{35}O_2^-$ (m/z = 283) (Fig. 7), respectively) but some other characteristic fragments are also identified in Fig. 8. They are $C_6H_4O_2Al^-$ (m/z = 135) and $C_6H_5O_2Al_2^-$ (m/z = 163) for both C7-COOH and C17-COOH. These fragments, not observed on the reference sample, correspond to a fragment of the molecule bonded to one or two Al. A fragment bonded with a single Al can be associated with a monodentate complex on the Al surface, whereas a fragment bonded with two Al can correspond to either a μ_2-bonded monodentate or a bidentate complex. Due to substrate preparation, these inhibitors are probably bonded by the carboxylate group to the hydroxylated Al surface, through inner-sphere adsorption.[53] Condensation is the mechanism invoked for the monodentate bond, by recombination of hydroxyl surface group with the COOH acidic proton and release of a water molecule.[54] Conversely, protonation of a surface OH group and the release of a second water molecule is necessary before the carbonyl group can react with Al and form the bidentate bonding mode.[54] Note that the ions correspond only to a fraction of the inhibitor molecule linked with Al. This may be due to the ToF–SIMS process itself, which reduces the probability of big ions emission. Thus, only fragments of the molecule linked with Al are observed.

Figure 9 displays specific fragments corresponding to the C8-Bn-COOH inhibitor linked with an Al, i.e. $C_7H_3O_2Al^-$ (m/z = 146), $C_7H_4O_2Al^-$ (m/z = 147), $C_7H_3O_2Al_2^-$ (m/z = 173) and $C_7H_4O_2Al_2^-$ (m/z = 174). They correspond to an aromatic cycle (that may lack one H atom) + carboxylate functional group bonded to one or two Al, respectively. This evidences the formation of carboxylate complexes when the hydroxylated surface is exposed to the C8-Bn-COOH inhibitor, with the same mechanism as explained for R-COOH.

Concerning the C8-PO(OH)$_2$ and C18-PO(OH)$_2$ inhibitors, the mass spectra (Fig. 10) also evidence fragments, i.e. $C_4H_5PO_3Al_2^-$ (m/z = 186), $C_4H_6PO_3Al_2^-$ (m/z = 187), $C_3H_4PO_3Al_3^-$ (m/z = 200) and $C_3H_6PO_3Al_3^-$ (m/z = 202), which correspond to a fragment of molecule bonded to two Al or three Al. It is noteworthy that no fragment bonded to only one Al is observed. This indicates that these inhibitors are bonded to the surface via the phosphonate group. The adsorption mechanism (chemisorption) suggested in the literature consists of a covalent bond formed by a condensation reaction between the PO(OH)$_2$ group of the inhibitor and surface hydroxyl groups.[53,55] Two condensation reactions lead to two strong PO–Al bonds (bidentate complex). To form a tridentate complex, the formation of the third PO–Al bond is required.[56,57] According to
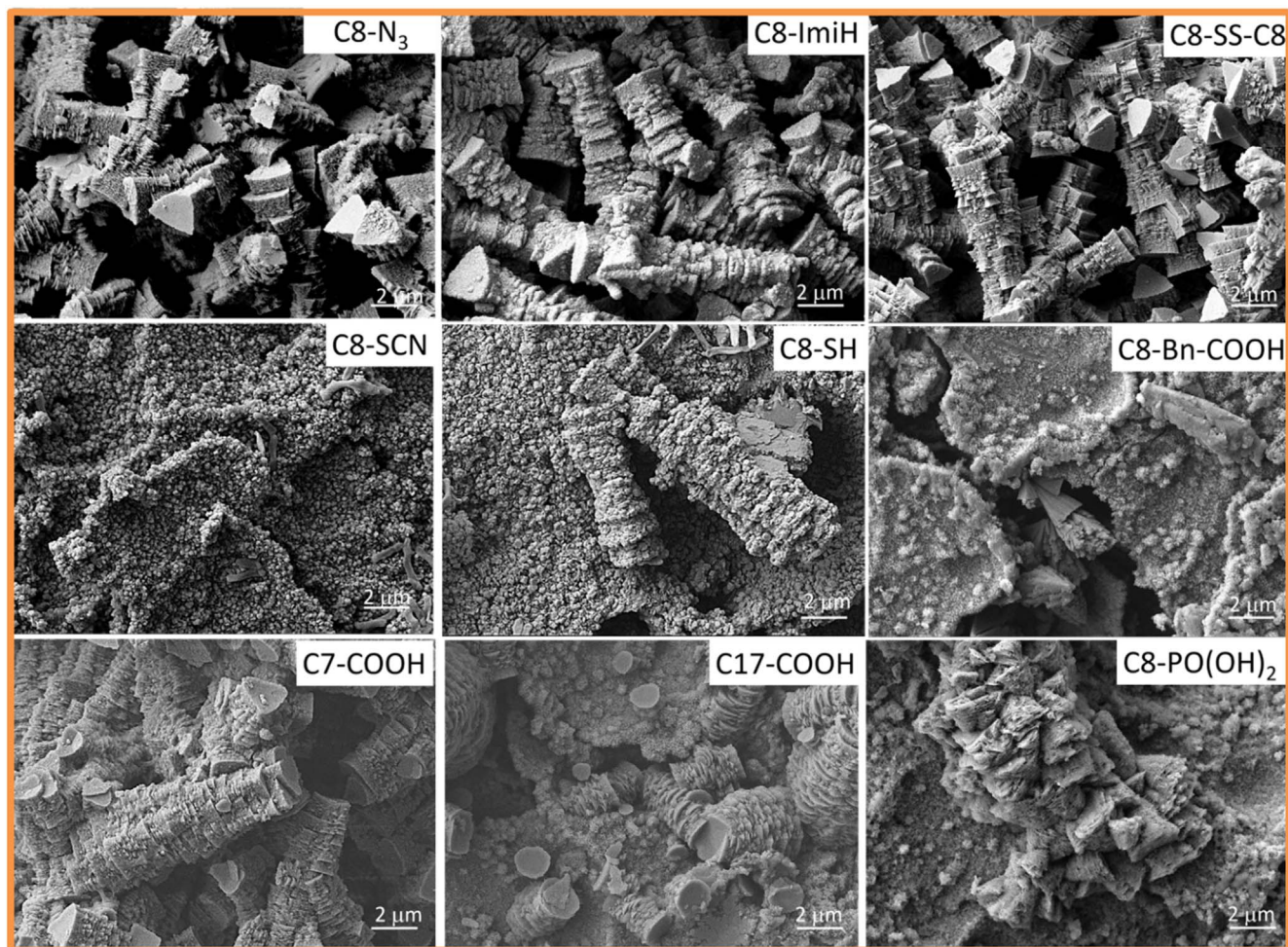
Figure 6. SEM images recorded at the surface alkaline etched Al samples modified by octyl and octadecyl alkyl chain with various anchor groups after immersion in 0.5 M NaCl for 6 months. LEI images were recorded at 5 kV and 5,000× magnification. The following surfaces were superhydrophilic before and after the test: C8-N3, C8-ImiH, C8-SS-C8, C8-SCN, C8-SH, and C7-COOH. The C8-Bn-COOH surface was hydrophobic and that of C17-COOH and C8-PO(OH)$_2$ superhydrophobic before the test and hydrophobic after the test.
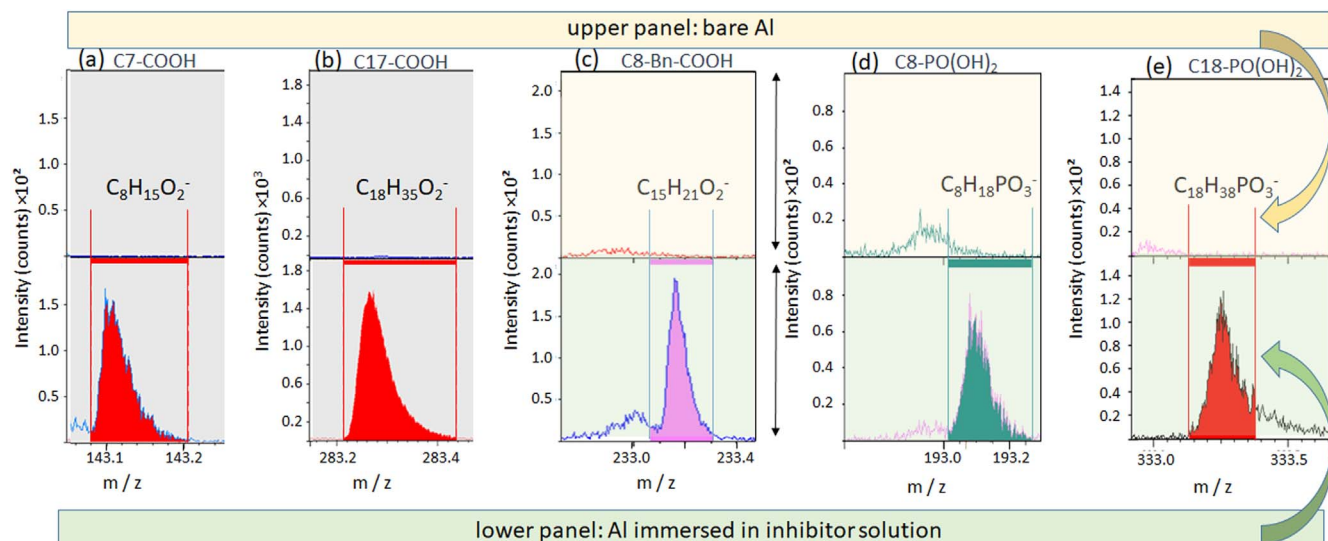

Figure 7. ToF-SIMS negative ion spectra obtained on (upper panel, yellow background) alkaline etched Al and (lower panel, green background) alkaline etched Al immersed for 30 min in 5 mM ethanol solution of (a) C7-COOH, (b) C17-COOH, (c) C8-Bn-COOH, (d) C8-PO(OH)$_2$ and (e) C18-PO(OH)$_2$. Spectra with a grey background, shown in (a, b), were published previously.[1]
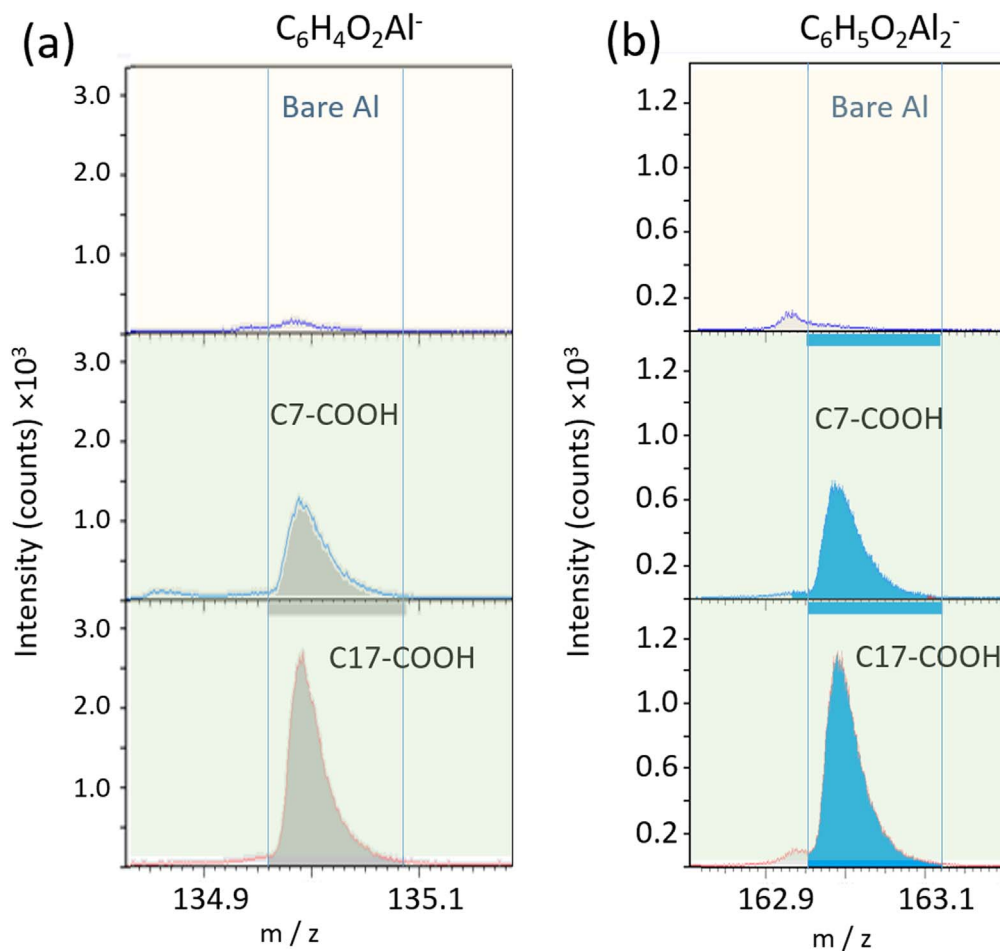
Figure 8. ToF-SIMS negative ion spectra showing C7-COOH and C17-COOH (a) monodentate and (b) bidentate carboxylate complex bonded to the alkaline etched Al surface.
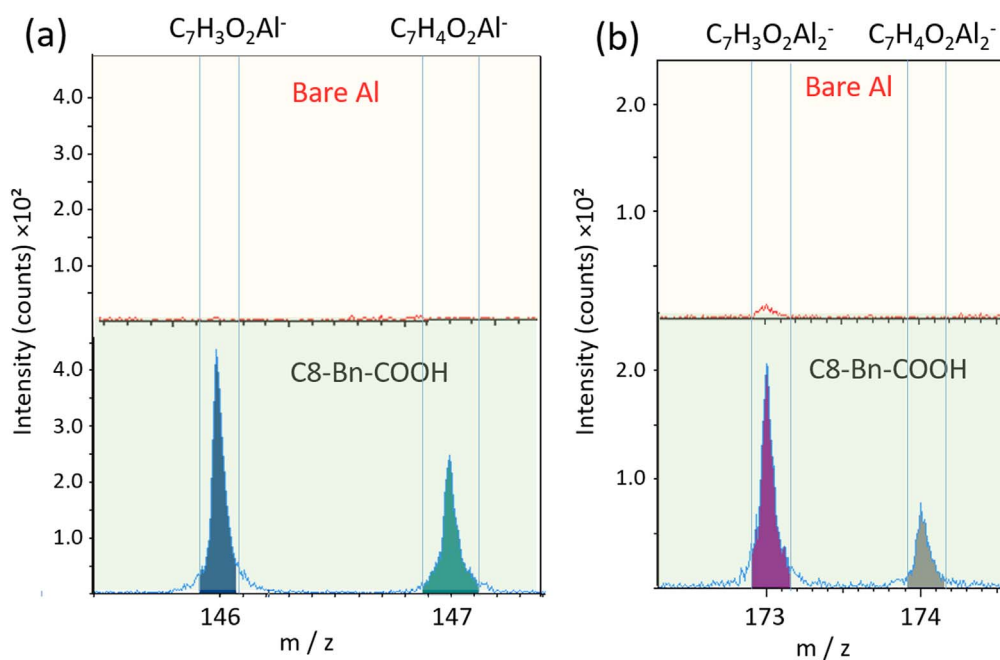

Figure 9. ToF-SIMS negative ion spectra showing C8-Bn-COOH (a) monodentate and (b) bidentate carboxylate complex bonded to the alkaline etched Al surface.
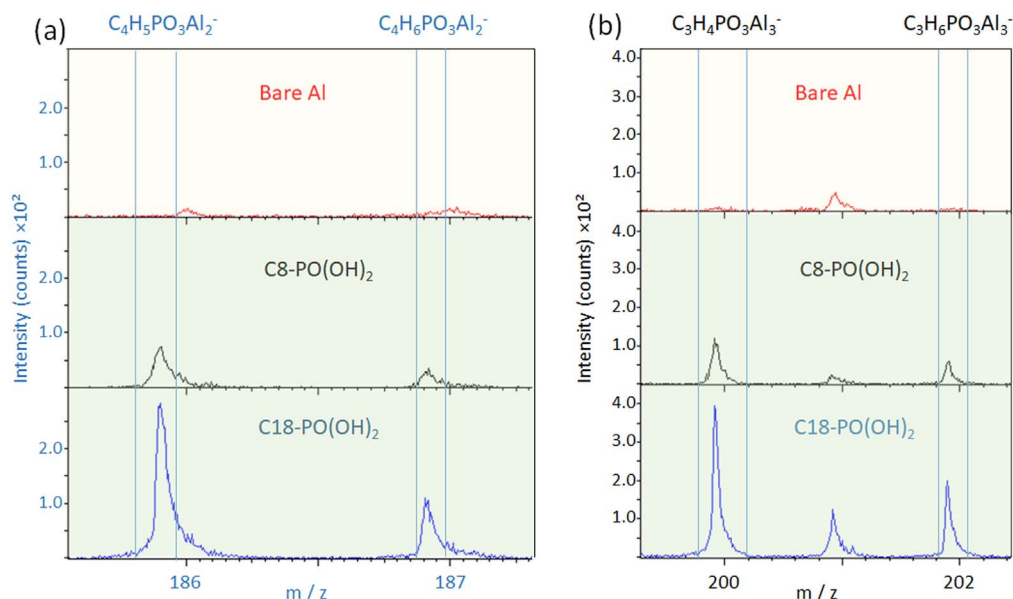
Figure 10. ToF-SIMS negative ion spectra showing C8-PO(OH)$_2$ and C18-PO(OH)$_2$ (a) bidentate and (b) tridentate phosphonate complex bonded to the alkaline etched Al surface.

Ramsier et al.,[58] for such a bond to form the P=O group needs to react with an unsaturated Al atom on the surface. Luschtinetz et al.[59] explained that in acidic medium a protonation of an OH group of the Al surface could release a water molecule, permitting a free Al site and so the third bond resulting from the coordination of the phosphoryl oxygen to the metal can form.[60]

ToF–SIMS/XPS analyses revealed the presence of all the tested compounds (three carboxylic acids and two phosphonic acids) on Al substrates exposed to their solutions. As schematically depicted in Fig. 11, carboxylic acids are bonded with the carboxylate group to the Al surface by one (monodentate) and two (μ_2-monodentate or bidentate) Al, while phosphonic acids are bonded by two (μ_2-monodentate or bidentate) and three Al (μ_1 + μ_2-bidentate or bidentate). In contrast, compounds with thiol, amine, imidazole, thiocyanate and azide functional groups are not present on the surface in sufficient amount to be detected by XPS; this implies that these compounds are not good candidates for corrosion inhibitors for Al.

Computational modeling.—In order to provide additional information on the adsorption affinity of various anchor groups on the oxidized aluminum surface, we performed the corresponding PBE–D$_0$

calculations. To this end, we divided the structure of the inhibitor molecules into two structural components: (i) an anchor group, which governs adhesion to the surface, and (ii) a backbone, responsible for lateral cohesive interactions within the adsorbed layer. A schematic representation of this structural division is shown in Fig. 12. To better disentangle anchor−surface adhesion from lateral cohesive effects of the backbone, a methyl group was used as a minimal backbone representation and calculations were performed at low molecular coverage (i.e. one molecule per (4 × 4) surface supercell).

We modeled the adsorption of a subset of the selected anchor groups (listed in Fig. 13) on the OH/Al$_x$O/Al(111) model of the hydroxylated oxidized aluminum surface, described in the Computational details section and shown in Fig. 13. XPS and ToF–SIMS results (shown in Figs. 4, 5, 7–10) indicate that some among the investigated molecules remain on the surface for an extended period of time (at least six months), which implies that these molecules are strongly chemisorbed. Hydrogen bonds between a molecule and a surface together with dative $X \rightarrow$ Al bonds (X = N, O, S) cannot provide so strong chemisorption, because, according to our calculations, the resulting magnitudes of adsorption energy are at most about 1 eV.[61] Thus a chemical reaction is required in order to
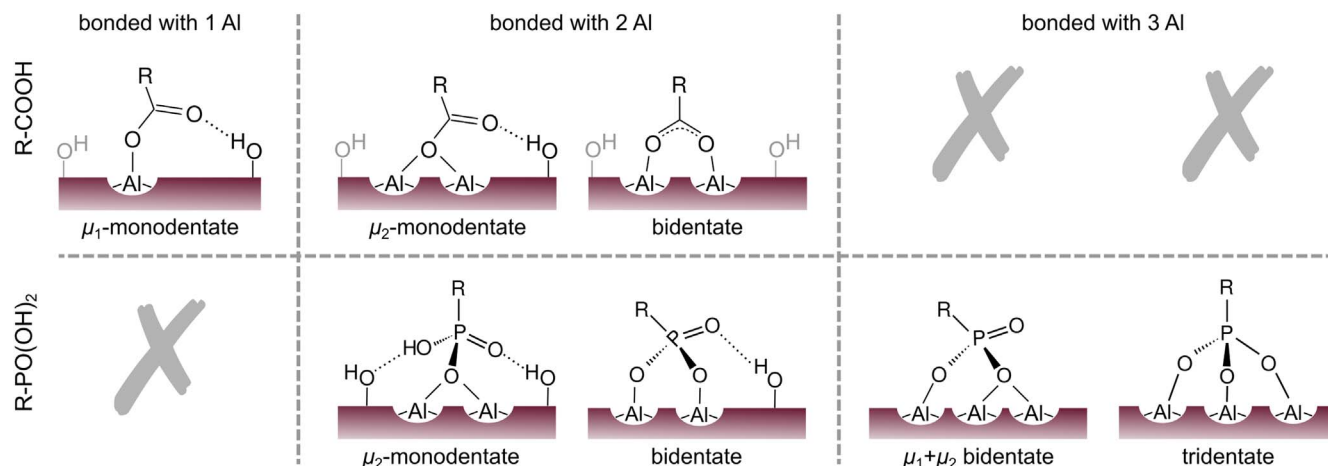

Figure 11. According to the ToF-SIMS fragment analysis, carboxylic acids bond to either one or two Al, whereas phosphonic acids bond to either two or three Al. Several potential bonding modes corresponding to these findings are schematically depicted (only the more probable modes as inferred from our DFT calculations are shown). Gray crosses indicate that the particular bonding mode is not compatible with the ToF-SIMS fragment analysis.
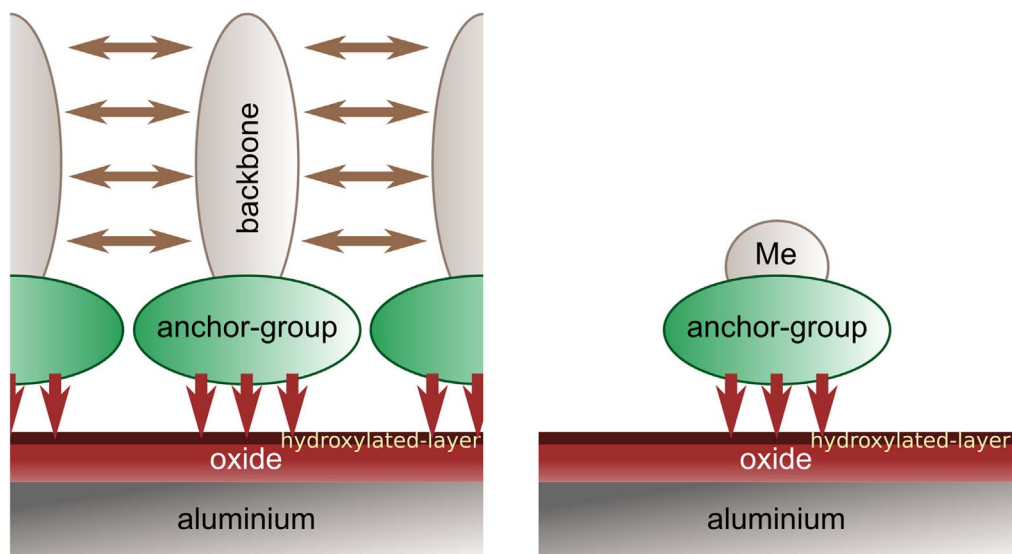
Figure 12. Schematic representation of the structural division of the inhibitor into an anchor group and a backbone (left). The anchor group governs adhesion to the surface (indicated by red arrows), whereas the backbone is responsible for cohesive interactions within the monolayer (brown arrows). In order to better disentangle the effects of the two structural components, a standalone adsorbed molecule with a methyl (Me) group as a minimal backbone (right) was used when investigating the effect of the anchor group.
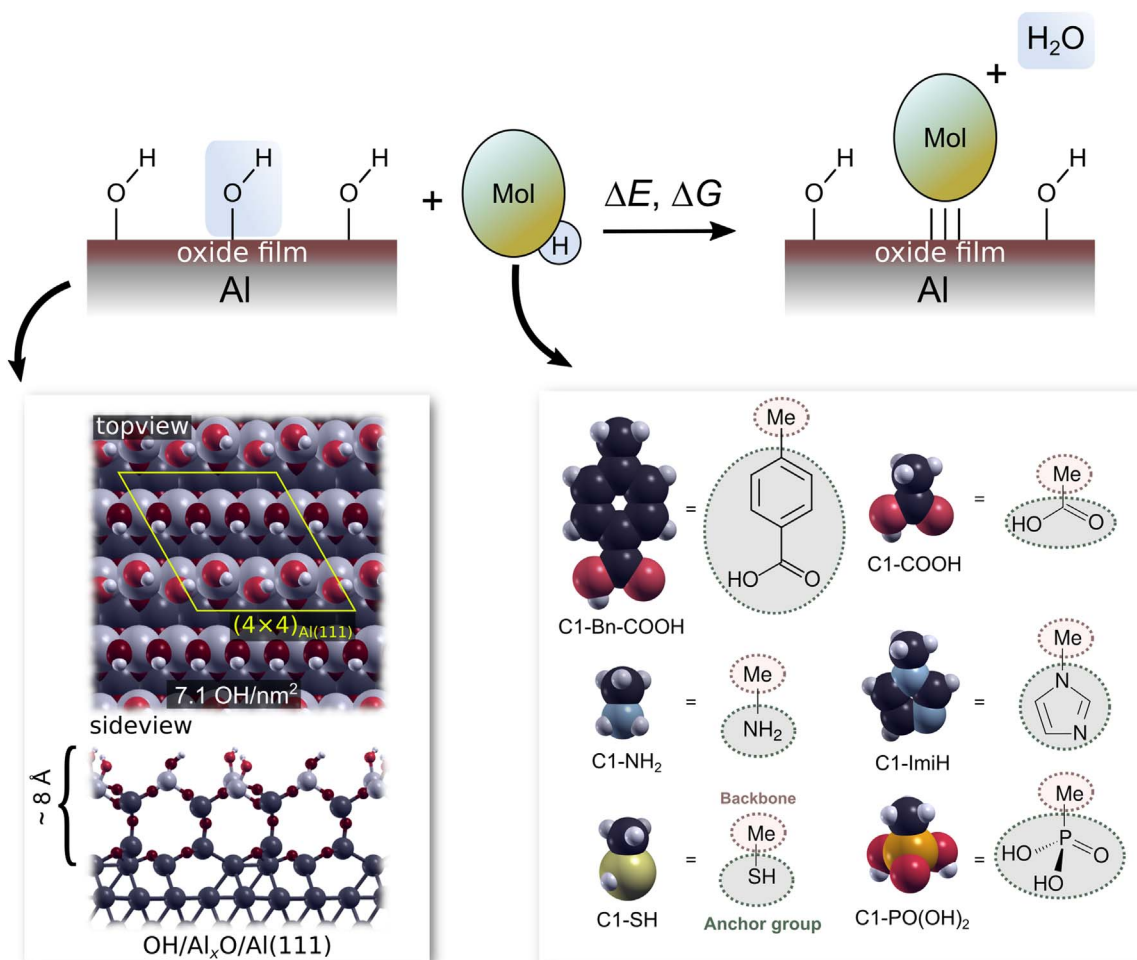
Figure 13. A scheme of the condensation reaction mechanism (top), where MolH is used as a generic label for the considered anchor groups. Below the scheme on the left-hand side the top- and side-view of the employed OH/Al$_x$O/Al(111) model of the hydroxylated oxidized aluminum surface are shown, whereas the different considered anchor groups are depicted on the right-hand side with methyl group used as a minimal representation of the backbone.
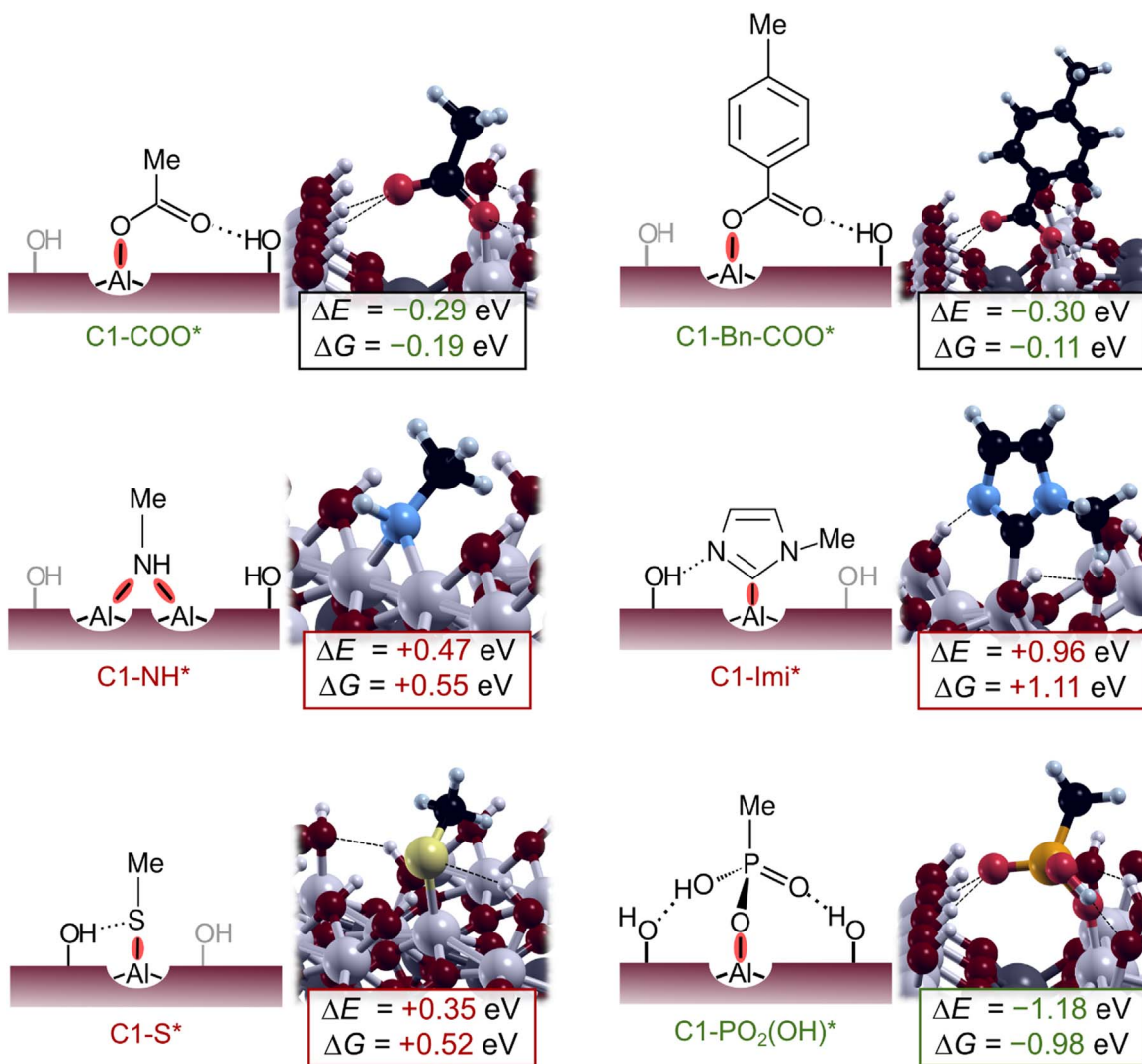
Figure 14. Schematic skeletal representation of the anchor–surface bonding as deduced from DFT calculations along with the corresponding snapshots of the optimized structures on the OH/Al$_x$O/Al(111) model. The calculated reaction energies (ΔE) and reaction free energies (ΔG) are also given for the condensation reaction of the considered anchor groups on the oxidized aluminum surface.

form stronger ionocovalent X–Al bonds (X = C, N, O, or S), with bond strengths up to 5 eV. We have previously shown that on the hydroxylated oxidized aluminum surface such bonds can form via the condensation mechanism,[1,20,24,25] which can be described by the reaction:

$$MolH + OH^* \rightarrow Mol^* + H_2O, \qquad [4]$$
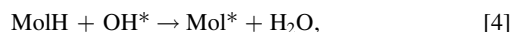
where the label MolH stands for the intact standalone molecule in the gas phase, Mol* represents the dissociated molecule adsorbed on the surface, and OH* is a surface hydroxyl group. The condensation reaction involves the dissociative adsorption of a molecule by replacing a surface OH group and forming a water molecule as a side product. This reaction is schematically shown in Fig. 13, along with the top- and side-view of the OH/Al$_x$O/Al(111) model of the hydroxylated oxidized aluminum surface and the considered anchor groups with a methyl group as a minimal backbone.

The results of our calculations are shown in Fig. 14. Only COOH and PO(OH)$_2$ anchor groups display exothermic ΔE values, being about -0.3 eV for C1-COOH and C1-Bn-COOH and -1.2 eV for C1-PO(OH)$_2$, whereas all others anchor groups display significantly endothermic reaction energies. It should be noted that although the magnitudes of ΔE values are moderate, below about 1 eV, the corresponding molecules–surface bonds are strong (from 3.8 eV for

S–Al to 5 eV for O–Al). The reason is that ΔE value does not reflect the chemisorption bond strength, because it is the cumulative effect of bond-breaking and bond-making.

To further corroborate the feasibility of the condensation adsorption reaction, we also calculated the corresponding reaction Gibbs free energies, ΔG at 298 K and 1 atm. It should be noted that all ΔG values, reported in Fig. 14, are less exergonic than ΔE values are exothermic. This is mainly due to the loss of roto-translational degrees of freedom upon adsorption, even though a water molecule is released during the reaction. However, the water molecule is less massive than all considered anchor groups (note that roto-translational entropic contributions are roughly proportional to the logarithm of the molecular mass).[b] Of the considered anchor groups, the

---

[b]The ideal-gas translational partition function is $q_{tr} = \left(\frac{mkT}{2\pi\hbar^2}\right)^{\frac{3}{2}} V$, where m is the mass of the molecule, k is the Boltzmann constant, T is the temperature, and V is the volume per ideal-gas particle. For a non-linear molecule, the rotational partition function is $q_{rot} = \frac{1}{\sigma_{rot}} \frac{\sqrt{8\pi^3(kT)^3 I_A I_B I_C}}{\hbar^3}$, where σ_{rot} is the rotational symmetry number, and I_A, I_B, and I_C are the three eigenvalues of the moment of inertia tensor, which depends on the mass distribution within the molecule. The corresponding entropies are $S_{tr} = k \ln(q_{tr} + 5/2)$ and $S_{rot} = k \ln(q_{rot} + 3/2)$, which implies that roto-translational entropic contributions are roughly proportional to the logarithm of the molecular mass (for an example that this is indeed the case see Fig. 16b of our parallel publication[20]).

most exergonic reaction free energy is found for C1-PO(OH)$_2$, with a ΔG of -0.98 eV. Both anchor groups containing the carboxylic functional group, C1–COOH and C1-Bn-COOH, display an only slightly exergonic ΔG of -0.19 eV and -0.11 eV, respectively, due to the mentioned unfavorable entropic effects. This indicates that additional stabilization is required for the formation of a stable carboxylate layer on the surface, which can be provided by cohesive lateral interactions between alkyl backbones within the adsorbed monolayer.[1,20] The remaining anchor groups all display considerably endergonic reaction free energies. The respective ΔG values for C1-SH, C1-NH$_2$, and C1-ImiH, are 0.52, 0.55, and 1.11 eV, which indicate that these molecules will not chemisorb via the condensation mechanism on the hydroxylated oxidized aluminum surface.

Let us also remark that these results agree remarkably well with XPS and ToF–SIMS measurements presented in Figs. 4, 5, 7–10, where molecules containing PO(OH)$_2$ and COOH anchor groups were identified on the surface, whereas the other anchor groups were not found. The modeling results are also in line with electrochemical measurements (*vide infra*, Figs. 18–19), where inhibitors containing the PO(OH)$_2$ anchor group were found to be efficient regardless the alkyl chain length. Additionally, the shorter-chain C8-COOH did not show inhibition characteristics, whereas the longer-chain C17-COOH was an efficient inhibitor, as already discussed in our previous publication.[1]

Our calculations also demonstrate that it is more appropriate to classify the benzene group of Bn-COOH as a backbone rather than an anchor group. From Fig. 14 it is evident that the chemisorption bonding of both standalone C1-COO* and standalone C1-Bn-COO* is similar, with condensation reaction energies of -0.3 eV. On the other hand, the ΔE values for the full monolayer of C1-COO* and C1-Bn-COO* are considerably different, being -0.15 and -0.64 eV molecule^{-1}, respectively (see Fig. 15). Thus the ΔE value for the full monolayer of C1-Bn-COO* is closer to that of C8-COO*, which has a value of -0.61 eV molecule^{-1}. The difference between the ΔE values of C1-COO* and C1-Bn-COO* monolayers also provides a rationale for the observed difference in inhibition efficiency of C8-Bn-COO* and C8-COO*, which will be discussed in the following section. Namely, in the light of considering the benzene group of Bn-COOH as a backbone, the C8-Bn-COOH would correspond to Cn-COOH with n being larger than 8. This reasoning is supported by the wettability measurements which show that C8-COOH is superhydrophilic, whereas C8-Bn-COOH is hydrophobic (Table I), in accordance with the increasing number of C atoms in the backbone.[1]

The above computational results refer exclusively to the formation of a monodentate bonding mode on the OH/Al$_x$O/Al(111) model via the condensation mechanism. However, the fragment analysis of the ToF–SIMS spectra indicates that inhibitors containing the COOH anchor group can bond also to two Al, which corresponds, according to Fig. 11, either to μ_2-monodentate or bidentate bonding modes. While according to DFT calculations standalone μ_1-monodentate is more stable than standalone μ_2-monodentate, a full monolayer consists of both types of monodentates.[20] As for the PO(OH)$_2$ anchor group, the ToF–SIMS analysis reveals that it bonds with either two or three Al. The fragment with two Al corresponds, according to Fig. 11, either to μ_2-monodentate or bidentate, whereas the fragment with three Al corresponds to $\mu_1 + \mu_2$-bidentate or tridentate. With DFT calculations we identified μ_2-monodentate, but it is by 0.15 eV less stable than the μ_1-monodentate, shown in Fig. 14. In contrast to ToF–SIMS, DFT calculations did not identify any structure, where the PO(OH)$_2$ anchor group bonds with three Al on a fully hydroxylated surface. For this reason, we investigated bidentate bonding of COOH and PO(OH)$_2$ headgroups and tridentate bonding of PO(OH)$_2$ on surface models that contain OH vacancies; vacancy containing models were treated as spin-polarized. These calculations indicate that bidentate configurations are viable near OH vacancies. In particular, on the OH/Al$_x$O/Al(111) model, monodentate bonded carboxylate and phosphonate stabilize by 0.66 and 0.90 eV, respectively, if they transform to the bidentate

configuration by bonding with the O atom of the C=O or P=O group to the Al ion that lacks the hydroxyl group (see Fig. 16). These results were obtained analogously to those of Fig. 14, i.e., calculations were performed at low molecular coverage with a methyl group used as a minimal backbone representation.

It should be noted that for the PO(OH)$_2$ headgroup the monodentate to bidentate transformation can proceed via two different routes. The first route is the one just considered, which can be written as:

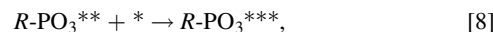$$R\text{-PO}_2(\text{OH})^* + ^* \rightarrow R\text{-PO}_2(\text{OH})^{**}, \qquad [5]$$
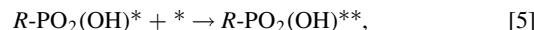
where a standalone * indicates a free adsorption site (in this case an OH vacancy), whereas the suffix * and ** designate monodentate and bidentate bonding, that is, bonding to one and two Al ions, respectively. The number of suffix asterisks also indicates the number of PO−Al bonds. The second route proceeds via the condensation mechanism:

$$R\text{-PO}_2(\text{OH})^* + \text{OH}^* \rightarrow R\text{-PO}_3^{**} + \text{H}_2\text{O}. \qquad [6]$$

This implies that the phosphonate headgroup can, in principle, form two stoichiometrically different bidentates with the surface, R-PO$_2$(OH)** and R-PO$_3$**. These two bidentates can then transform to tridentates via the following reactions:

$$R\text{-PO}_2(\text{OH})^{**} + \text{OH}^* \rightarrow R\text{-PO}_3^{***} + \text{H}_2\text{O} \qquad [7]$$

and

$$R\text{-PO}_3^{**} + ^* \rightarrow R\text{-PO}_3^{***}, \qquad [8]$$

where *** indicates tridentate bonding with the surface or, alternatively, three PO−Al bonds. Note that a water molecule is liberated in reactions 6 and 7, hence for their proper thermodynamic characterization, calculations of reaction free energies are required, given that the roto-translational contribution of a released water molecule to the Helmholtz free energy is -0.51 eV (calculated value) at room temperature and 1 atm. In contrast, reactions 5 and 8 can be approximately described by reaction energies, because no new species is immobilized or liberated.

Reactions 5 to 8 were modeled on two different surface models, OH/Al$_x$O/Al(111) and Al(OH)$_3$(010), and both contain one OH vacancy per supercell. The corresponding results, obtained at low molecular coverage with a methyl group used as a minimal backbone, are presented in Fig. 17. This figure schematically presents the reactions 5 to 8 along with reaction (free) energies and the snapshots of identified bidentate and tridentate structures. Two surface models were used in order to diminish model induced biases. The results indicate that transformation of phosphonate monodentate to bidentate is viable only near an OH vacancy via reaction 5 with the reaction energies ($\Delta E_{\text{mono}\rightarrow\text{bi}}$) of -0.90 and 0.02 eV on OH/Al$_x$O/Al(111) and Al(OH)$_3$(010) models, respectively. In contrast, the transformation from monodentate to R–PO$_3$** bidentate via the condensation mechanism, reaction 6, is found considerably endothermic on both surface models; also the corresponding reaction free energies are endergonic, the values being 0.68 and 0.37 eV on OH/Al$_x$O/Al(111) and Al(OH)$_3$(010), respectively.

As for the transformation of bidentate to tridentate, the two surface models differ greatly. While this transformation is endothermic and endergonic on the OH/Al$_x$O/Al(111) model, it is exergonic on Al(OH)$_3$(010), irrespectively of the path taken. Cumulatively, reaction free energies of monodentate to tridentate transformation are $+0.88$ and -0.39 eV on OH/Al$_x$O/Al(111) and Al(OH)$_3$(010) models with an OH vacancy, respectively. This implies that, according to DFT calculations, formations of bidentates and tridentates are viable, but only near OH vacancies. In particular, the formation of tridentate is viable on the Al(OH)$_3$(010) model with the OH vacancy, whereas the OH/Al$_x$O/Al(111) model supports only the formation of bidentate via reaction 5 near the OH vacancy.

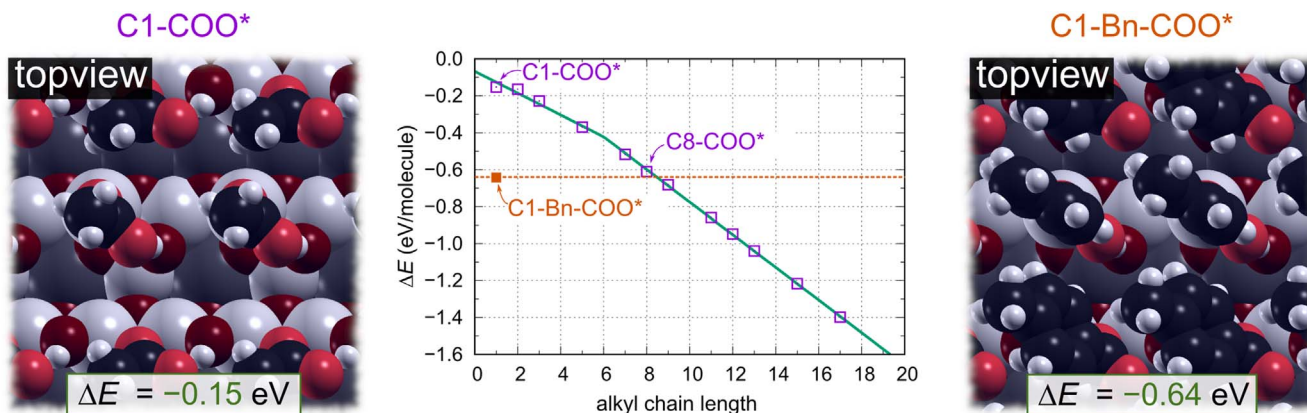**Figure 15.** The dependence of ΔE of a full monolayer of Cn-COO* on alkyl chain length n (purple squares) and the ΔE for the full monolayer of C1-Bn-COO* (orange square). The ΔE of C1-Bn-COO* monolayer is closer to that of C8-COO* than to C1-COO*, which indicates that the benzene group of Bn-COO* acts more as a backbone than an anchor group; note that C1-Bn contains 7 C atoms. The snapshots of the C1-COO* and C1-Bn-COO* monolayers are shown on the left and right, respectively. The ΔE values for the monolayers of Cn-COO* are taken from our parallel publication and correspond to the OH/Al$_x$O/Al(111) model.[20]

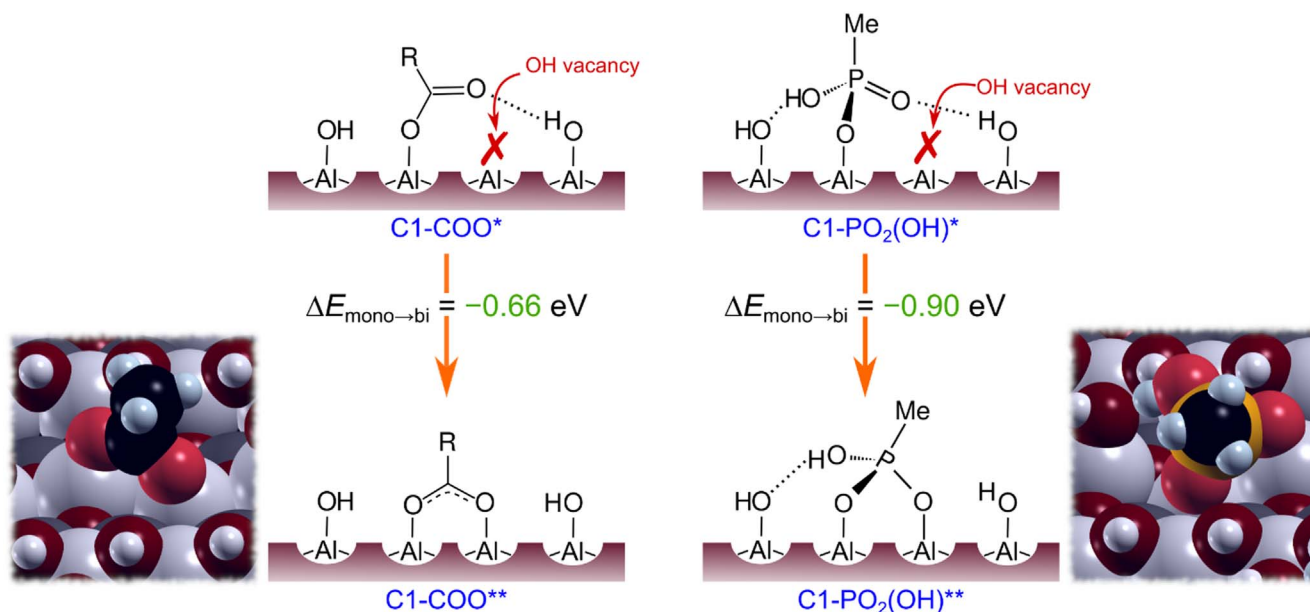**Figure 16.** A scheme showing the transformation of monodentate bonded C1-COO* (left) and C1-PO$_2$(OH)* (right) into C1-COO** and C1-PO$_2$(OH)** bidentates on the OH/Al$_x$O/Al(111) model with an OH vacancy defect; the number of the suffix * indicates the number of CO−Al or PO−Al bonds. The snapshots of the resulting bidentates are also shown on the far left and right. Monodentate to bidentate transformation reaction energies ($\Delta E_{\text{mono}\rightarrow\text{bi}}$), calculated with spin-polarized calculations, are also given.

Electrochemical properties of etched aluminum modified with alkyl compounds with various anchor groups.—Potentiodynamic polarization curves in 0.5 M NaCl were recorded for bare etched Al and etched Al samples immersed for 30 min in 5 mM ethanol solution of different organic chemicals with C8 alkyl chain and various anchor groups (N$_3$, ImiH, NH$_2$, SS, SH, SCN, COOH, Bn-COOH and PO(OH)$_2$) (Fig. 18). The polarization curve of alkaline etched Al, recorded in 0.5 M NaCl after 1 h under open circuit condition, shows the cathodic curve related to the reduction of oxygen and the anodic curve to dissolution of Al.[62] The corrosion potential (E_{corr}) was located at −0.78 V, and corrosion current density (j_{corr}) was 3.05 μA cm^{-2} (Table II).

All samples pre-immersed in ethanol solution of C8-R or C18-R compounds show different curves than the etched sample, indicating that the presence of adsorbed organic layer affects the electrochemical response of Al samples. Electrochemical parameters deduced from polarization curves are presented in Table II. C8-SS-C8 and, especially, C8-N$_3$ are the only compounds which act as corrosion

activators with j_{corr} larger than that of bare etched Al. All other compounds act as mixed corrosion inhibitors as they caused the reduction of current density in both cathodic and anodic regions leading to overall reduction in corrosion current density compared to that of bare etched Al (3.05 μA cm^{-2}). Among C8–R compounds, roughly three groups could be distinguished according to the current density and shape of the curve: (i) COOH, SCN and SH with j_{corr} above 1 μA cm^{-2} but being up to two times smaller than for the bare etched Al, (ii) NH$_2$, Bn-COOH and ImiH with j_{corr} reduced by about one order of magnitude ($j_{\text{corr}} < 0.5$ μA cm^{-2}), and (iii) PO(OH)$_2$ with $j_{\text{corr}} \approx 0.1$ μA cm^{-2} and a pseudo-passive range, which is defined as a plateau region in which the current density remains constant or increases very slowly with increasing potential; it is limited by the breakdown potential at which current density increases abruptly, i.e. $\Delta E_{\text{passive}} = |E_{\text{break}} - E_{\text{corr}}|^c$. For

---

^{c}Please note that the $\Delta E_{\text{passive}}$ is taken arbitrarily as a passive range since it denotes the range between breakdown potential and corrosion potential, and not between breakdown potential and potential of passivation.
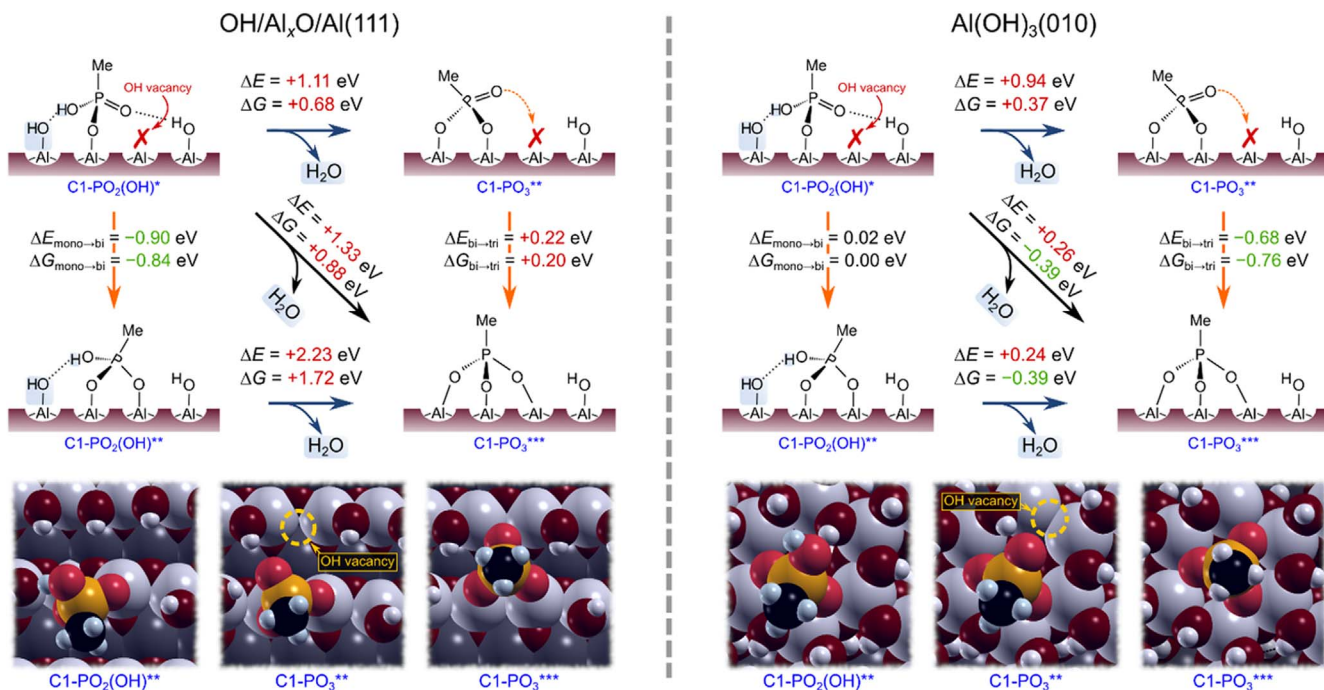
Figure 17. Reaction schemes for monodentate to tridentate transformations of the phosphonate headgroup on $OH/Al_xO/Al(111)$ (left) and $Al(OH)_3(010)$ (right) surface models containing one OH vacancy per supercell. Two different reaction paths (via two different bidentates) are considered: the upper path proceeds first with the condensation reaction step and then with the plain transformation and vice-versa for the bottom path. The corresponding reaction energies (at 0 K) and reaction free energies (at 298 K and 1 atm), calculated with spin-polarized calculations, are also given. ΔE and ΔG correspond to condensation reaction steps, whereas $\Delta X_{mono \to bi}$ and $\Delta X_{bi \to tri}$ ($X \equiv E$ or G) correspond to plain monodentate to bidentate and plain bidentate to tridentate transformations, respectively. Snapshots of the most stable identified bidentates and tridentates are shown in the bottom row panels.
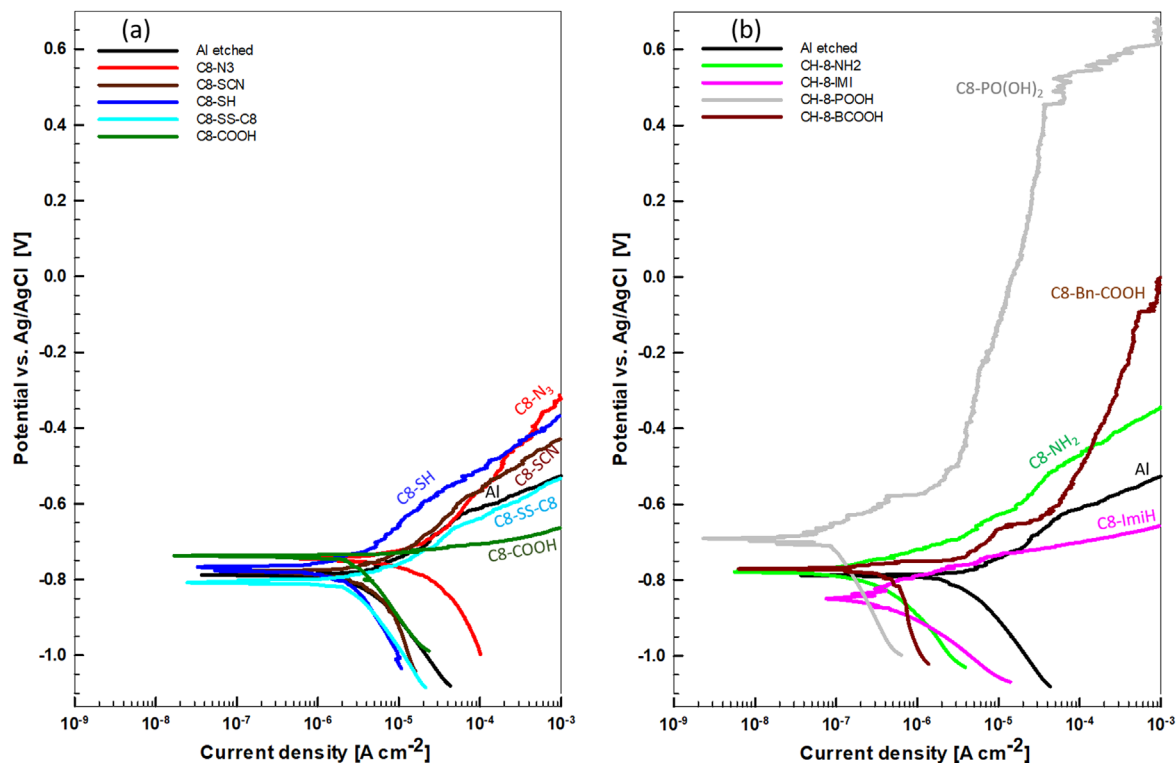

Figure 18. Potentiodynamic polarization curves recorded in 0.5 M NaCl or alkaline etched Al with and without prior immersion for 30 min in 5 mM ethanol solution of organic compounds with octyl alkyl chain and various anchor groups: (a) azide N_3, thiocyanate SCN, thiol SH, disulphide SS, and carboxylic COOH, and (b) amino NH_2, imidazole ImiH, phosphonic $PO(OH)_2$ and benzoic Bn-COOH. The rest time under open circuit conditions was 1 h. The scan rate was 1 mV s^{-1}. Electrochemical parameters are presented in Table II.

Table II. Electrochemical parameters (corrosion current density (j_{corr}), corrosion potential (E_{corr}), breakdown potential (E_{break}) and $\Delta E_{passive} = |E_{break} - E_{corr}|$) deduced from potentiodynamic polarization curves (Figs. 18 and 19) recorded for etched Al (labelled as Al) or etched Al samples covered by organic layer (labelled as Cx-R) where x is the number of carbon atoms in the alkyl chain ($x = 8$ or 18) and R is the anchor group as defined in Fig. 1. Al was etched for 20 min in 0.1 M NaOH at 90 °C, cooled down in the same solution, and then immersed in 5 mM ethanol solution of organic chemical. Results are presented as mean ± standard deviation.

| Sample/Type of organic chemical	$j_{corr}/\mu A\ cm^{-2}$	E_{corr} vs Ag/AgCl/V	E_{break} vs Ag/AgCl/V	$\Delta E_{passive}$/V
Al	3.05 ± 0.21	−0.74 ± 0.01	—	—
		C = 8		
C8-N$_3$	15.05 ± 3.61	−0.75 ± 0.01	—	—
C8-SS-C8	4.35 ± 2.61	−0.80 ± 0.003	—	—
C8-COOH	2.24 ± 0.53	−0.75 ± 0.01	—	—
C8-SCN	2.10 ± 1.13	−0.78 ± 0.008	—	—
C8-SH	1.37 ± 1.17	−0.80 ± 0.04	—	—
C8-NH$_2$	0.45 ± 0.11	−0.77 ± 0.005	—	—
C8-Bn-COOH	0.29 ± 0.18	−0.77 ± 0.004	—	—
C8-ImiH	0.22 ± 0.02	−0.83 ± 0.02	—	—
C8-PO(OH)$_2$	0.11 ± 0.003	−0.66 ± 0.05	0.36 ± 0.13	1.20
		C = 18		
C18-SH	3.82 ± 2.00	−0.79 ± 0.001	—	—
C17-COOH	0.07 ± 0.01	−0.63 ± 0.05	0.54 ± 0.13	1.17
C18-PO(OH)$_2$	0.08 ± 0.00	−0.69 ± 0.08	1.29 ± 0.24	1.98
C18-ImiH	3.75 ± 0.28	−0.77 ± 0.006	—	—
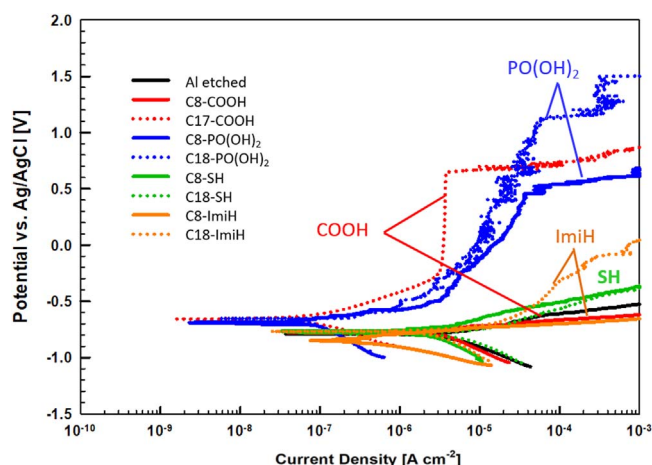
Figure 19. Potentiodynamic polarization curves recorded in 0.5 M NaCl for alkaline etched Al without and with subsequent immersion for 30 min in 5 mM ethanol solution of organic compounds with octyl (solid) and octadecyl (dotted) alkyl chains and various anchor groups: thiol SH, imidazole ImiH, carboxylic COOH and phosphonic PO(OH)$_2$. The resttime under open circuit conditions was 1 h. The scan rate was 1 mV s^{-1}. Electrochemical parameters are presented in Table II.

C8-PO(OH)$_2$ the value of $\Delta E_{passive}$ is about 1.2 eV; the benzoic group also showed some tendency for pseudo-passivity. The reduction of current density is similar on both more noble (cathodic) and less noble (anodic) sides. E_{corr} was either up to 50 mV more cathodic (Bn-COOH, SCN, NH$_2$, SH, SS and ImiH), or up to 140 mV more anodic (N$_3$, COOH and PO(OH)$_2$) compared to the bare sample. Based on these results it can be stated that compounds with the C8 chain and COOH, SCN, SH, NH$_2$, Bn-COOH and ImiH anchor groups act as weak to moderate mixed inhibitors. C8-PO(OH)$_2$ acts as a mixed barrier inhibitor with a strong effect on the anodic side showing barrier properties.

For four anchor groups—COOH, SH, ImiH and PO(OH)$_2$—the effect of chain length on corrosion current density was investigated. Polarization curves recorded for bare etched Al and etched Al samples immersed in organic chemicals with the C18 alkyl chain and four anchor groups are presented in Fig. 19. The deduced

electrochemical parameters are presented in Table II. For the sake of comparison, curves recorded for Al modified with C8 chain with same anchor groups are repeated herein. Elongation of the alkyl chain with the SH group from C8 to C18 did not contribute to increased protectiveness of the surface, and j_{corr} was even larger than for the octyl chain and bare etched Al. A similar situation is encountered for the imidazole group with the difference that in the anodic range the increase in current density was lower. When the C18 chain is bonded to COOH and PO(OH)$_2$ groups the elongation of the alkyl chain is beneficial and results in the establishment of a broad pseudo-passivity region with $\Delta E_{passive}$ of 1.17 V and 1.98 V, respectively. In both cases j_{corr} was below 0.1 $\mu A\ cm^{-2}$ (Table II).

Based on these results it can be stated that thiol and imidazole groups were not protective regardless the length of alkyl chain, the carboxylic group was protective for the longer (C18) chain, and the phosphonic group was protective regardless of the length of alkyl chain. These experimental electrochemical results confirm the surface-analytical results (Figs. 4, 5, 7–10) and computational results presented in Figs. 13–17.

Conclusions

1. Thirteen alkyl-based organic compounds were purposely prepared to study the effect of anchor group and alkyl chain length on adsorption on a superhydrophylic, hydroxylated aluminum surface. The study was tackled on four levels: (i) synthesis or purchase of appropriate organic compounds, (ii) fabrication of adsorbed organic layers on Al etched in alkaline NaOH solution; (iii) their experimental characterization using electrochemical and surface-analytical (SEM/EDS, XPS, and ToF–SIMS) techniques; and (iv) DFT modeling of adhesion and self-assembly of organic layers on oxidized Al substrates.

2. Based on electrochemical results, nine anchor groups—azide, imidazole, thiocyanate, amino, disulfide, thiol, phosphonic, carboxylic and benzoic—bonded to an octyl alkyl chain (C8-R) can be divided into three groups: (i) corrosion activators (azide and disulfide), (ii) not inhibitors or weak to moderate inhibitors (carboxylic, thiocyanate, thiol, amino, benzoic and imidazole) and (iii) strong inhibitors (phosphonic). When bonded to a longer, octadecyl alkyl chain (C18-R), imidazole and thiol groups remained weak inhibitors, the phosphonic group remained a strong inhibitor, and the carboxylic acid became a strong inhibitor. In other words, thiol and imidazole

groups were not protective regardless the length of alkyl chain, the carboxylic group was protective for the longer chain, and the phosphonic group was protective regardless of the length of alkyl chain. The mode of inhibition is mixed with a strong effect on the anodic side reflecting in a broad pseudo-passivity region of over 1 V. At the same time, the wettability of the surface changes: when bonded to the C8 alkyl chain, all anchor groups form superhydrophilic layers on the Al surface except the phosphonic group which forms a superhydrophobic layer; when bonded to the C18 alkyl chain, carboxylic and phosphonic layers are superhydrophobic.

3. XPS analysis was used as a finger-print for the adsorption of organic compounds and the formation of dense molecular layers on aluminum surface. It was found that carboxylic and phosphonic anchor groups are firmly bonded to the etched Al surface, whereas other tested anchor groups, containing nitrogen or sulfur, are not. ToF-SIMS/XPS analysis was then explored to analyze the bonding mechanism: carboxylic acids are bonded with the carboxylate group to either one or two surface Al, while phosphonic acids are bonded to either two or three surface Al. These molecules remain on the surface for an extensive period of time (at least six months), which implies that they are strongly chemisorbed.

4. To further corroborate the adsorption affinity of various anchor groups for the hydroxylated/oxidized aluminum surface, DFT calculations were performed at low molecular coverage with a methyl group used as a minimal backbone. Given that experiments show that some anchor groups strongly chemisorb, adsorption was modeled via the condensation reaction mechanism. Among the considered anchor groups only COOH, Bn-COOH, and PO(OH)$_2$ display exergonic reaction free energies with the last anchor group being the most strongly chemisorbed. The respective reaction adsorption free energies are −0.19, −0.11, and −0.98 eV (at room temperature and 1 atm). These values imply that for carboxylic anchor groups additional stabilization is required to form stable molecular layers: this stabilization can be provided by lateral cohesive interactions between alkyl chains but only if the chains are long enough. This explains why C17-COOH forms denser molecular layers than C8-COOH and consequently why the former is a better inhibitor than the latter. DFT calculations also suggest that it is more appropriate to classify the benzene group of Bn-COOH as a backbone rather than an anchor group, which is why the performance of C8-Bn-COOH as a corrosion inhibitor is in between that of C8-COOH and C17-COOH.

5. As for the question of bidentate bonding of carboxylic anchor groups as well as bidentate and tridentate bonding of phosphonic anchor group, DFT calculations suggest that such bonding modes are viable only near OH vacancies. In contrast, on fully hydroxylated surfaces without OH vacancies, we were not able to identify bidentate bonded carboxylate, whereas the monodentate to bidentate transformation of phosphonate was found to be endergonic.

6. The integrative experimental-modeling approach applied on the targeted system *Al-surface/anchor group/alkyl backbone* brought about valuable information concerning the mechanism of interaction of various anchor groups with Al. Our next study will concentrate on the system *Al-surface/anchor group/perfluoro backbone*.

Acknowledgments

ORCID

I. Milošev ⓘ https://orcid.org/0000-0002-7633-9954
Ch. Carriére ⓘ https://orcid.org/0000-0002-1796-7539
J. Iskra ⓘ https://orcid.org/0000-0001-6340-3577
S. Stavber ⓘ https://orcid.org/0000-0002-0850-6511
M. Poberžnik ⓘ https://orcid.org/0000-0002-4866-4346
A. Kokalj ⓘ https://orcid.org/0000-0001-7237-0041
P. Marcus ⓘ https://orcid.org/0000-0002-9140-0047

References

1. I. Milošev et al., "Electrochemical, surface-analytical, and computational DFT study of alkaline etched aluminum modified by carboxylic acids for corrosion protection and hydrophobicity." *J. Electrochem. Soc.*, **166**, C3131 (2019).
2. D. Winkler, "Predicting the performance of organic corrosion inhibitors." *Coatings*, **7**, 553 (2017).
3. S. A. Umoren and M. M. Solomon, "Synergistic corrosion inhibition effect of metal cations and mixtures of organic compounds: a review." *J. Environ. Chem Eng.*, **5**, 246 (2017).
4. European Chemical Agency ECHA, (2017), DOI: https://doi.org/10.2823/470616.
5. A. Kokalj and D. Costa, "Molecular modeling of corrosion inhibitors." *Reference Module in Chemistry, Molecular Sciences and Chemical Engineering; Encyclopedia of Interfacial Chemistry: Surface Science and Electrochemistry'* (Elsevier, Amsterdam) Vol. 6.1, p. 332 (2018).
6. S. Sharma, X. Ko, Y. Kurapati, H. Singh, and S. Nešić, "Adsorption behaviour of organic corrosion inhibitors on metal surfaces—some new insights from molecular dynamics simulations." *Corrosion*, **75**, 90 (2019).
7. C. D. Taylor, "Molecular modeling of structure and reactivity at the metal/ environment interface." *Molecular Modeling of Corrosion Processes: Scientific Development and Engineering Applications*, ed. C. D. Taylor and P. Marcus (Wiley) The Electrochemical Society Series (Pennington, NJ) (2015).
8. C. D. Taylor, "Corrosion informatics: an integrated approach to modeling corrosion." *Corros. Eng. Sci. Technol.*, **50**, 490 (2014).
9. A. Kokalj, "Is the analysis of molecular electronic structure of corrosion inhibitors sufficient to predict the trend of their inhibition performance." *Electrochim. Acta*, **56**, 745 (2010).
10. D. A. Winkler, M. Breedon, P. White, A. E. Hughes, E. D. Sapper, and I. Cole, "Using throughput experimental data and *in silico* models to discover alternatives to toxic chromate corrosion inhibitors." *Corros. Sci.*, **106**, 229 (2016).
11. K. Xanari and M. Finšgar, "Organic corrosion inhibitors for aluminium and its alloys in chloride and alkaline solutions: a review." *Arab. J. Chem.*, **12**, 4646 (2016).
12. G. T. Hefter, N. A. North, and S. H. Tan, "Organic corrosion inhibitors in neutral solutions; inhibitions of steel, copper, and aluminium by straight chains carboxylates." *Corrosion*, **53**, 657 (1997).
13. A. Kokalj, S. Peljhan, M. Finšgar, and I. Milošev, "What determines the inhibition efficiency of ATA. BTAH and BTAOH corrosion inhibitors on copper?" *J. Am. Chem. Soc.*, **132**, 16657 (2010).
14. I. Milošev, N. Kovačević, J. Kovač, and A. Kokalj, "The roles of mercapto, benzene and methyl groups in the corrosion inhibition of imidazoles on copper: I. Experimental characterization." *Corros. Sci.*, **98**, 107 (2015).
15. N. Kovačević, I. Milošev, and A. Kokalj, "The roles of mercapto, benzene and methyl groups in the corrosion inhibition of imidazoles on copper: II. Inhibitor−copper bonding." *Corros. Sci.*, **98**, 457 (2015).
16. D. S. Chauhan, M. A. Quraishi, C. Carrière, P. Marcus, and A. Singh, "Electrochemical, ToF-SIMS and computational studies of 4-amino-5-methyl-4H-1,2,4-triazole-3-thiol as a novel corrosion inhibitor for copper in 3.5% NaCl." *J. Mol. Liq.*, **289**, 111113 (2019).
17. C. Monticelli, "Corrosion inhibitors." *Encyclopedia of Interfacial Chemistry, Surface Science and Electrochemistry* (Elsevier, Amsterdam) p. 164 (2018).
18. E. Kálmán, F. H. Kármán, J. Telegdi, B. Várghegyi, J. Balla, and T. Kiss, "Inhibition efficiency on N-containing carboxylic and carboxy-phosphonic acids." *Corros. Sci.*, **35**, 1477 (1993).
19. R. Zhao, P. Rupper, and S. Gaan, "Recent development in phosphonic-acid based organic coatings on aluminium." *Coatings*, **7**, 133 (2017).
20. M. Poberžnik, F. Chiter, I. Milošev, P. Marcus, D. Costa, and A. Kokalj, "DFT study of *n*-alkyl carboxylic acids on oxidized aluminum surfaces: from standalone molecules to self-assembled-monolayers." *Appl. Surf. Sci.* (2020).

21. L. Liu, X. Feng, and M. Guo, "Eco-friendly fabrication of superhydrophobic bayerite array on Al foil via an etching and growth process." *J. Phys. Chem.*, **117**, 25519 (2013).

22. R. Viroulaud, J. Świątowska, A. Seyeux, S. Zanna, J. Tardelli, and P. Marcus, "Influence of surface pretreatments on the quality of trivalent chromium process coatings on aluminium alloy." *Appl. Surf. Sci.*, **423**, 927 (2017).

23. M. Ely, J. Świątowska, A. Seyeux, S. Zanna, and P. Marcus, "Role of post-treatment in improved corrosion behavior of trivalent chromium protection (TCP) coating deposited on aluminum alloy 2024-T3." *J. Electrochem. Soc.*, **164**, C276 (2017).

24. D. Costa, T. Ribeiro, P. Cornette, and P. Marcus, "DFT modeling of corrosion inhibition by organic molecules: carboxylates as inhibitors of aluminum corrosion." *J. Phys. Chem. C*, **120**, 28607 (2016).

25. M. Poberžnik, D. Costa, A. Hemeryck, and A. Kokalj, "Insight into the bonding of silanols to oxidized aluminum surfaces." *J. Phys. Chem. C*, **122**, 9417 (2018).

26. V. N. Emel'yanenko, M. Algarra, J. C. G. Esteves da Silva, J. Hierrezuelo, J. M. López-Romero, and S. P. Verevkin, "Thermochemistry of organic azides revisited." *Thermochim. Acta*, **597**, 78 (2014).

27. A. A. Salman, M. Tabandeh, T. Heidelberg, R. S. D. Hussen, and H. M. Ali, "Alkyl-imidazolium glycosides: non-ionic—cationic hybrid surfactants from renewable resources." *Carbohyd.Res.*, **412**, 28 (2015).

28. R. J. Capon, C. Skene, E. Hasang-Te Liu, E. Lacey, J. H. Gill, K. Heiland, and T. Friedel, "Nematocidal thiocyanatins from a Southern Australian Marine Sponge Oceanapia sp." *J. Nat. Prod.*, **67**, 1277 (2004).

29. Y. Ju, D. Kumar, and R. S. Varma, "Revisiting nucleophilic substitution reactions: microwave-assisted synthesis of azides, thiocyanates, and sulfones in an aqueous medium." *J. Org. Chem.*, **71**, 6697 (2006).

30. A. Ghavdast, N. O. Mahmoodi, and M. A. Zanjanchi, "Synthesis and photochromic properties of disulfide-1,3-diazabicyclo [3.1. 0] hex-3-ene functionalized silver nanoparticles." *J. Mol. Liq.*, **198**, 128 (2014).

31. H. Firouzabaddi, N. Iranmpoor, and M. Abbasi, "A one-pot, efficient, and odorless synthesis of symmetrical disulfides using organic halides and thiourea in the presence of manganese dioxide and wet polyethylene glycol (PEG-200)." *Tetrahedron Lett.*, **51**, 508 (2010).

32. M. Tosoni, S. Laschat, and A. Baro, "Synthesis of novel chiral ionic liquids and their phase behavior in mixtures with smectic and nematic liquid crystals." *Helv. Chim. Acta*, **87**, 2742 (2004).

33. N. J. Shirtcliffe, G. McHale, S. Atherton, and M. I. Newton, "An introduction to superhydrophobicity." *Adv. Colloid Interfac.*, **161**, 124 (2010).

34. J. H. Scofield, "Hartree-Slater subshell photoionization cross-sections at 1254 and 1487 eV." *J. Electron Spectrsc. Relat. Phenom.*, **8**, 129 (1976).

35. S. Tanuma, C. J. Powell, and D. R. Penn, "Calculations of electron inelastic mean free paths. II. Data for 27 elements over the 50–2000 eV range." *Surf. Interface Anal.*, **17**, 911 (1991).

36. P. Giannozzi et al., "Quantum ESPRESSO: a modular and open-source software project for quantum simulations of materials." *J. Phys.: Condens. Matter*, **21**, 395502 (2009).

37. P. Giannozzi et al., "Advanced capabilites for materials modeling with Quantum ESPRESSO." *J. Phys.: Condens. Matter*, **29**, 465901 (2017).

38. J. P. Perdew, K. Burke, and M. Ernzerhof, "Generalized gradient approximation made simple." *Phys. Rev. Lett.*, **77**, 3865 (1996).

39. D. Vanderbilt, "Soft self-consistent pseudopotentials in a generalized eigenvalue formalism." *Phys. Rev. B*, **41**, 7882 (1990).

40. Ultrasoft pseudopotentials for H, C, N, O, Al, P and S atoms were taken from the Quantum ESPRESSO Pseudo Potential Download Page: http://quantum-espresso. org/pseudopotentials (files: H.pbe-rrkjus.UPF, C.pbe-rrkjus.UPF, N.pbe-rrkjus. UPF, O.pbe-rrkjus.UPF, Al.pbe-n-rrkjus_psl.0.1.UPF, P.pbe-n-rrkjus_psl.0.1.UPF, S.pbe-n-rrkjus_psl.0.1.UPF) (2019).

41. S. Grimme, "Semiempirical GGA-Type density functional constructed with a long-range dispersion correction." *J. Comput. Chem.*, **27**, 1787 (2006).

42. M. Methfessel and A. T. Paxton, "High-precision sampling for Brillouin-zone integration in metals." *Phys. Rev. B*, **40**, 3616 (1989).

43. A. Kokalj, "XCrySDen–a new program for displaying crystalline structures and electron densities." *J. Mol. Graph. Model.*, **17**, 176 (1999).

44. M. Poberžnik and A. Kokalj, "Implausibility of bidentate bonding of the silanol headgroup to oxidized aluminium surfaces." *Appl. Surf. Sci.*, **492**, 909 (2019).

45. C. Lanthony, J. Ducéré, M. D. Rouhani, A. Hemeryck, A. Estève, and C. Rossi, "On the early stage of aluminum oxidation: an extraction mechanism via oxygen cooperation." *J. Chem. Phys.*, **137**, 094707 (2012).

46. S. Baroni, S. de Gironcoli, A. Dal Corso, and P. Giannozzi, "Phonons and related crystal properties from density-functional perturbation theory." *Rev. Mod. Phys.*, **73**, 515 (2001).

47. R. F. Ribeiro, A. V. Marenich, C. J. Cramer, and D. G. Truhlar, "Use of solution-phase vibrational frequencies in continuum models for the free energy of solvation." *J. Phys. Chem. B*, **115**, 15556 (2011).

48. T. Tankam, K. Poochampa, T. Vilaivan, M. Sukwattanasintt, and S. Wacharasindhu, "Organocatalytic visible light induced S–S bond formation for oxidative coupling of thiols to disulfides." *Tetrahedron*, **72**, 788 (2016).

49. F. Teng, J. T. Yu, H. Yang, and J. Cheng, "A copper-mediated oxidative *N*-cyanation reaction." *Chem. Commun.*, **50**, 8412 (2014).

50. F. Schüler, B. Kerscher, F. Brecket, R. Thomann, and R. Mülhaupt, "Hyperbranched polymeric ionic liquids with onion-like topology as transporters and compartmentalized systems." *Angew. Chem.*, **52**, 455 (2013).

51. J. F. Moulder, W. F. Stickle, P. E. Sobol, and K. D. Bomben, *Handbook of X-ray Photoelectron Spectroscopy* (Perkin-Elmer Corp., Eden Prairie, MN) (1992).

52. A. Benninghoven, "Secondary ion mass spectrometry of organic compounds." *Secondary Ion Mass Spectrometry SIMS III*, ed. A. Benninghoven et al. (Springer, Berlin, Heidelberg) Vol. 19 Springer Series in Chemical Physics (1982).

53. S. P. Pujari, L. Scheres, A. T. M. Marcelis, and H. Zuilhof, "Covalent surface modification of oxide surfaces." *Angew. Chemie Int. Ed.*, **53**, 6322 (2014).

54. T. Bauer, T. Schmaltz, T. Lenz, M. Halik, B. Meyer, and T. Clark, "Phosphonate-and carboxylate-based self-assembled monolayers for organic devices: a theoretical study of surface binding on aluminum oxide with experimental support." *ACS Appl. Mater. Inter.*, **5**, 6073 (2013).

55. G. Guerrero, P. Hubert Mutin, and A. Vioux, "Organically modified aluminas by grafting and sol–gel processes involving phosphonate derivatives." *J. Mater. Chem.*, **11**, 3161 (2001).

56. P. J. Hotchkiss, S. C. Jones, S. A. Paniagua, A. Sharma, B. Kippelen, N. R. Armstrong, and S. R. Marder, "The modification of indium tin oxide with phosphonic acids: mechanism of binding, tuning of surface properties, and potential for use in organic electronic applications." *Acc. Chem. Res.*, **45**, 337 (2011).

57. L. Portilla, "Functionalization of metal oxide nanostructures via self-assembly. implications and applications." PhD thesisFaculty of Engineering, Friedrich-Alexander University(Erlangen-Nürnberg, Germany) (2017).

58. R. D. Ramsier, P. N. Henriksen, and A. N. Gent, "Adsorption of phosphorus acids on alumina." *Surf. Sci.*, **203**, 72 (1988).

59. R. Luschtinetz, R. A. F. Oliveira, J. Frenzel, J.-O. Joswig, G. Seifert, and H. A. Duarte, "Adsorption of phosphonic and ethylphosphonic acid on aluminum oxide surfaces." *Surf. Sci.*, **602**, 1347 (2008).

60. P. Hubert Mutin, G. Guerrero, and A. Vioux, "Hybrid materials from organophosphorus coupling molecules." *J. Mater. Chem.*, **15**, 3761 (2005).

61. M. Poberžnik, "Quantum mechanical modeling of the oxidation of aluminum surfaces and their interactions with corrosion inhibitors." PhD thesisUniversity of Ljubljana (2019).

62. R. Winston Revie, *Uhlig's Corrosion Handbook* (John Willey & Sons Inc, New York) 3rd ed. (2011).